JOURNAL OF GEOPHYSICAL RESEARCH, VOL. 97, NO. C7, PAGES 11,199–11,218, JULY 15, 1992

The Oceanography of Winter Leads

J. H. MORISON,[1] M. G. MCPHEE,[2] T. B. CURTIN,[3] AND C. A. PAULSON[4]

Leads in pack ice have long been considered important to the thermodynamics of the polar regions. A winter lead affects the ocean around it because it is a density source. As the surface freezes, salt is rejected and forms more dense water which sinks under the lead. This sets up a circulation with freshwater flowing in from the sides near the surface and dense water flowing away from the lead at the base of the mixed layer. If the mixed layer is fully turbulent, this pattern may not occur; rather, the salt rejected at the surface may simply mix into the surface boundary layer. In either event the instability produced at the surface of leads is the primary source of unstable buoyancy flux and, as such, exerts a strong influence on the mixed layer. Here as many as possible of the disparate and almost anecdotal observations of lead oceanography are assembled and combined with theoretical arguments to predict the form and scale of oceanographic disturbances caused by winter leads. The experimental data suggest the velocity disturbances associated with lead convection are about 1–5 cm s^{-1}. These appear as jets near the surface and the base of the mixed layer when ice velocities across the lead are less than about 5 cm s^{-1}. The salinity disturbances are about 0.01 to 0.05 psu. Scaling arguments suggest that the geostrophic currents set up by the lead density disturbances are also of the order of 1–5 cm s^{-1}. The disturbances are most obvious when freezing is rapid and ice velocity is low because the salinity and velocity disturbances in the upper ocean are not smeared out by turbulence. In this vein, lead convection may be characterized at one extreme as free convection in which the density disturbance forces the circulation. At the other extreme, lead convection may be characterized as forced convection in which the density disturbance is mixed rapidly by boundary layer turbulence. The lead number L_o, which is the ratio of the pressure term to the turbulence term in the momentum equation, and the turbulent lead number L_{ot}, which is the ratio of buoyant production to shear production in the turbulent kinetic energy equation, define the boundary between the free and forced regimes. For L_o and L_{ot} less than one, both the large-scale circulation and the turbulence are forced by surface stress. For L_o and L_{ot} greater than one, both the large-scale circulation and the turbulence are forced by the buoyancy flux. The magnitudes of velocity and salinity disturbances from a model developed elsewhere, suitable to free convection, agree with what few observations we have. The results of a forced convection model, developed here, suggest salinity disturbances of the order of 0.01–0.02 practical salinity units, with the maximum occurring at the surface of the lead and decreasing substantially below 5–10 m. This unstable gradient is a unique characteristic of lead convection. Though the salinity disturbances may be small when ice velocities are large, the buoyancy flux in leads has a major effect on the boundary layer turbulence.

1. INTRODUCTION

Leads in pack ice have long been considered important to the thermodynamics of the polar regions. *Badgley* [1966] estimated the total heat flux from the Arctic Ocean through leads to be equal in magnitude to the flux through the rest of the pack ice cover, even though leads account for only about 10% of the surface area. This is because the relatively warm ocean surface is exposed to the atmosphere directly or through a very thin layer of ice. *Maykut* [1978] has suggested that open leads, thin ice (<1.0 m) and thick ice (>1.0 m) contribute equally to the total heat flux. Usually, this flux is due to latent heat of fusion released during ice formation because the water under the ice is at the freezing point during fall, winter, and spring. Therefore the total amount of ice formed in leads is of the same magnitude as that formed under all the perennial ice. Also, because salt is rejected as sea water freezes, the freezing in leads accounts for a major fraction of the salt input to the arctic mixed layer.

Over the past 30 years there have been numerous lead observations. However, at least with regard to oceanographic measurements, most of these have been made on an opportunistic basis; that is, measurements were being made at ice camps for other purposes when a lead would open nearby and produce some noticeable effect on the ongoing measurements, or the field party would take what steps they could to make measurements near the lead. An exception was the 1974 AIDJEX Lead Experiment (ALEX). It was conducted as part of the Arctic Ice Dynamics Joint Experiment (AIDJEX) and involved near-surface atmospheric and oceanographic measurements at sites off Barrow, Alaska [*Paulson and Smith*, 1974]. From 1978 to 1980, *Topham et al.* [1983] made extensive measurements at a polynya near Dundas Island. They were able to make long-term measurements of the effect of the polynya on the atmospheric boundary layer because the polynya there is kept open by strong tidal currents. *Smith et al.* [1990] have given an excellent review of these and related studies, especially with regard to the atmospheric and ice observations.

In general, atmospheric boundary layer and ice growth studies, such as those of *Gow et al.* [1992], have been much more conclusive than the oceanographic studies. The reason for this is illustrated by the experience during ALEX. There the atmospheric research group and the oceanographic research group would attempt to fly out to a lead within 30 km of shore and set up their equipment rapidly on both sides of a lead before it closed or froze over. The atmospheric research group was usually able to set up and make detailed measurements quickly, owing to the lighter weight of their

[1]Polar Science Center, Applied Physics Laboratory, University of Washington, Seattle.
[2]McPhee Research, Naches, Washington.
[3]Office of Naval Research, Arlington, Virginia.
[4]College of Oceanography, Oregon State University, Corvallis.

Paper number 92JC00684.
0148-0227/92/92JC-00684$05.00

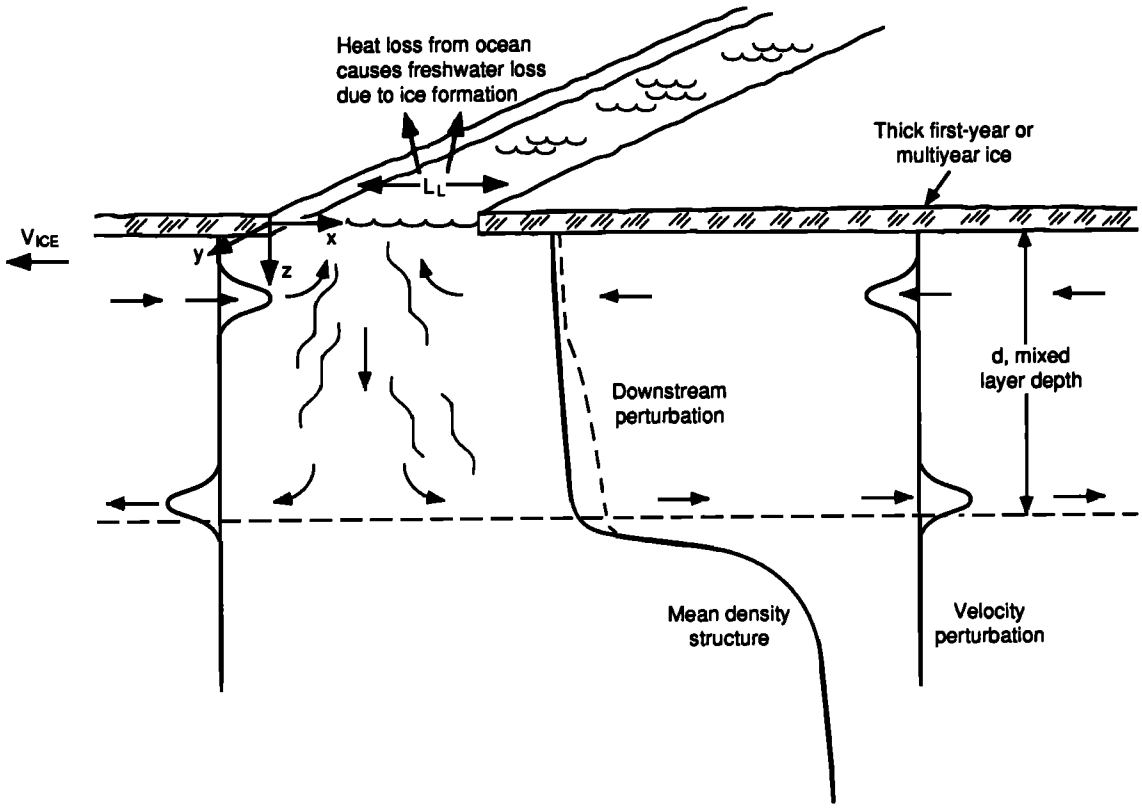

Fig. 1. A conceptual illustration of the circulation induced by a winter lead in the absence of rapid ice motion. Unstable buoyancy flux at the lead surface causes a high aspect ratio, cellular convection pattern with inflow near the surface and outflow near the base of the mixed layer.

instrumentation and the relative ease of setting it up on the surface. Drilling holes and deploying heavy equipment for the oceanographic experiments took longer, and the leads were at a more mature stage of development by the time measurements began. Further, it was found that useful atmospheric measurements could be made at an artificial lead made on the surface of an ice-covered lagoon.

In the literature there is little information about the oceanographic effects of leads because it is so difficult to make a concerted, complete set of oceanographic measurements near them. Most of the observations, considered singly and without a great deal of supporting data, do not give a coherent picture. However, individual observations have given rise to various ideas concerning wintertime lead-driven convection. After finding evidence of velocity jets immediately under the ice and at the base of the mixed layer, *Smith* [1973] proposed that buoyancy flux caused by brine rejection at the surface of a refreezing lead could drive a cellular circulation having a high aspect ratio. This is illustrated in Figure 1. The idea is that as the surface freezes, salt is rejected and forms more dense water which sinks under the lead. This sets up a circulation with freshwater flowing in from the sides near the surface and dense water flowing away from the lead at the base of the mixed layer. If the mixed layer is fully turbulent, this pattern may not occur; rather, the salt rejected at the surface may simply mix into the surface boundary layer. In either event the instability produced at the surface of leads is the primary source of unstable buoyancy flux and, as such, exerts a strong influence on the mixed layer. In contrast to open oceans and models of open ocean mixed layer dynamics, the buoyancy flux is concentrated in narrow bands, so understanding lead-driven convection is crucial to understanding polar mixed layer dynamics.

With the heightened interest in the relation of the polar oceans to climate change and atmosphere-ocean interactions, there is also a renewed interest in lead dynamics; several experiments related to leads and polynyas are being proposed. *Smith et al.* [1990] provide a great deal of useful background with which to plan this new generation of lead experiments, but they tend to emphasize the atmospheric boundary layer results, owing to the lack of published oceanographic results. For this reason it seems appropriate to assemble as many of the disparate and almost anecdotal observations of lead oceanography as possible and combine them with theoretical arguments to predict the form and scale of oceanographic disturbances caused by leads. This will provide a framework of key questions to be answered in future field work. In the following we will first present these observations, starting with a particularly serendipitous set of measurements taken when a lead opened through an established ice camp. Then a dimensional analysis will be presented in order to tie the different observations together and predict the scale of the disturbances caused by a single lead. Finally, model results will be examined to refine our estimates of the scale of these disturbances.

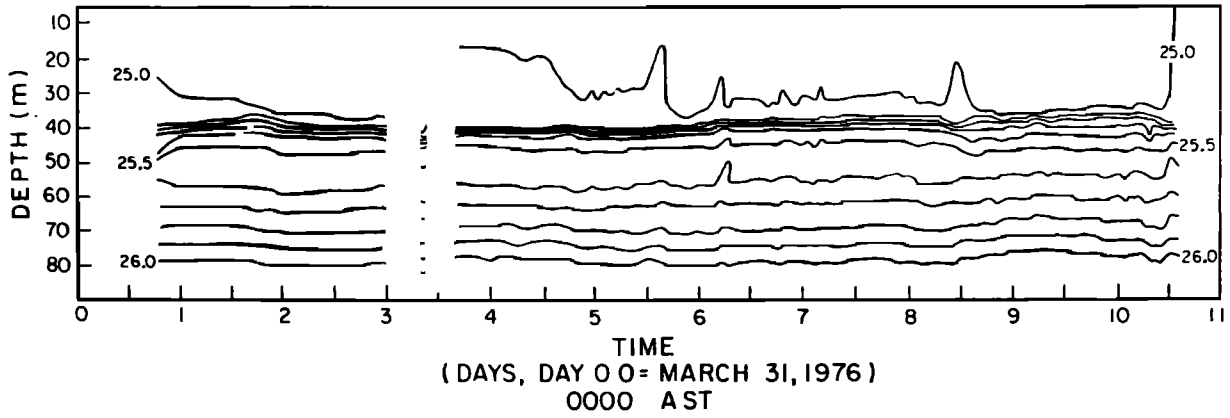

Fig. 2. Isopycnal depths at the Arctic Mixed Layer Experiment (AMLE) camp plotted versus time starting at midnight (AST) on March 31, 1976. The data gaps on day 3 are due to equipment problems.

2. Observations: "Lead Stories"

Lead Convection Observed During the Arctic Mixed Layer Experiment

In the ideal lead experiment, an ice camp equipped with oceanographic instrumentation would be established on an ice floe, and then, when all was ready, a lead would open through the camp. Our first example is in some respects like this ideal yet demonstrates many of the difficulties of interpreting measurements in the vicinity of rapidly freezing leads. Our intent here is to show a period of anomalous behavior in the upper ocean that coincided with the breakup of a drifting ice camp during the Arctic Mixed Layer Experiment (AMLE) and to ask whether local lead convection could have caused the observed behavior. We find the answer is equivocal; the data are limited in scope because safety required immediate evacuation. Thus, for example, we cannot immediately dismiss the argument that the station drifted across a preexisting frontal region at the time of breakup, causing the observed increase in mixed layer salinity. Nevertheless, there is enough information to show that under certain assumptions the lead could account for the change. The exercise illustrates many considerations that must go into a properly designed lead experiment, and the calculations lay the ground work for the scaling arguments to follow.

The AMLE was conducted in the Beaufort Sea at 73°N, 142°W from March 31 to April 10, 1976. The purpose was to measure the response of the ocean boundary layer and mixed layer under smooth ice. The experiment has been described by *Morison* [1980]. Equipment at the small camp included a profiling current meter-conductivity-temperature-depth (CTD) system, called the Arctic Profiling System (APS) [*Morison*, 1978], and two turbulence masts, suspended beneath the ice. The masts supported triads of small, ducted rotor current meters [*Smith*, 1978] with which to measure turbulence at fixed depths. The camp was established on a large refrozen lead covered with fairly smooth ice 1-m thick. With the exception of one storm on April 8, winds were calm during much of the experiment. Figure 2 shows isopycnal depths plotted versus time starting at midnight on March 31. (Time is given as local, that is, Alaska Standard Time (AST), in all the historical observations.) The two major disturbances during the experiment are apparent; the first, starting at about 1000 on April 8, has been interpreted by *Morison* [1980] as a forced internal wave response to the short storm. The disturbance that occurred after the lead opened at about 1200 on April 10 is in some ways more dramatic. Changes occurred throughout the upper 90 m, and the 25.0-σ_t isopycnal rapidly reached the surface for the first and only time in the experiment.

When the April 10 breakup occurred, the APS automatic winch was left to profile unattended, so CTD and velocity profile data were gathered from before the lead opened until over 3 hours later. Figure 3 is a rough map of the AMLE floe. It is based on notes in the camp log, personal recollection, and interpretation of photographs taken around 1500–1600 on April 10 and during evacuation on April 11. It shows the estimated orientation of the lead and the lead width estimated to be about 100 m at 1500–1600 on April 10. Figure 4 shows velocity and density profiles averaged over the last hour of operation along with a density profile obtained before the lead opened. The relative current velocity in the mixed layer from 1430 to 1530 was directed 20° (at 10 m) to 27° (at 30 m) true as indicated by the arrows in Figure 3. The lead as a whole was oriented approximately 20° true. Thus the currents were approximately aligned with the lead axis.

Changes in the density field were dramatic, mainly in the mixed layer. Figure 5 shows the changes in the upper ocean salinity at three depths plotted versus time. The salinity first increased at the deepest depths. The disturbance then moved up the water column, finally causing an increase in the mixed layer salinity starting at 1240. After this time the salinity at 20.5 m increased 0.07 practical salinity units (PSU), while the initial density disturbance at depth gradually decreased. Comparing the before and after density profiles of Figure 4 suggests the average mixed layer salinity increased about 0.05 PSU. A decrease in density at depths from 35 to 41 m was caused by the deepening and sharpening of the pycnocline. As will be shown, the decrease in salt content below 35 m can account for over a third of the increase in salinity above 35 m if it is assumed the salt is entrained into the mixed layer. The mixed layer deepening may have been due in part to turbulent mixing at the base of the mixed layer, caused by convection under the lead. The deepening and the disturbance below 40 m apparent in Figures 2 and 5 may also have been due to an internal wave response to buoyancy flux in the lead. *Morison* [1980] has

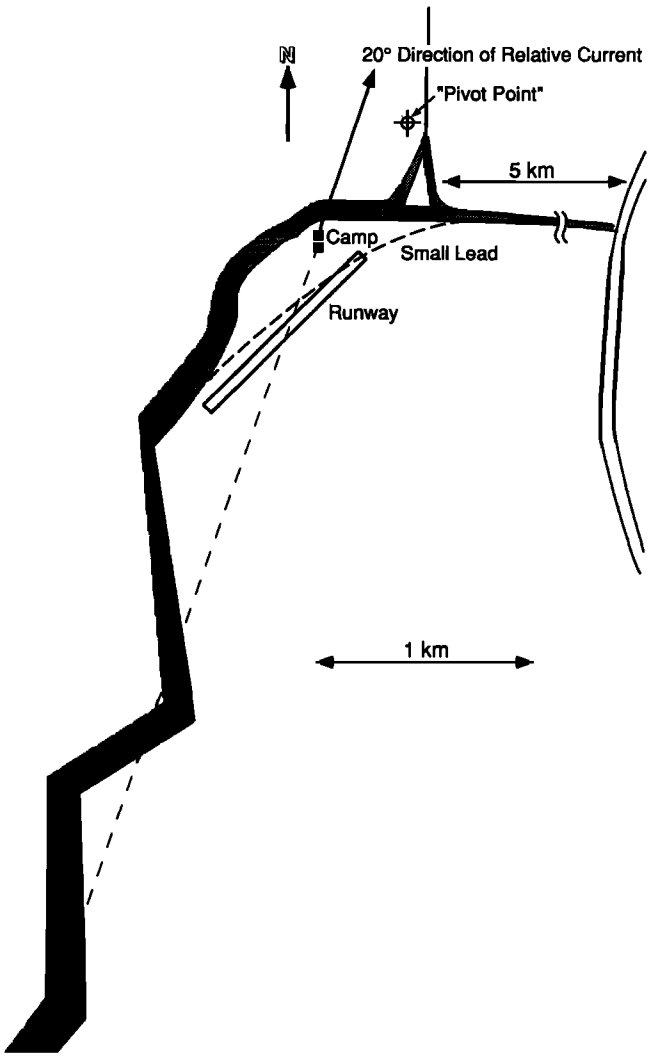

Fig. 3. Map of the AMLE floe based on notes in the camp log, personal recollection, and interpretation of photographs taken around 1500–1600 AST on April 10 and during evacuation on April 11. It shows the estimated orientation of the lead, and the lead width estimated to be about 100 m at 1500–1600 AST on April 10.

found that at scales appropriate to lead dynamics the internal wave response to buoyancy flux may be substantial, indeed, more important than that caused by surface stress variation. Recent numerical model results (D. C. Smith IV, personal communication, 1991) also suggest the internal wave response to buoyancy flux in the mixed layer can be substantial.

We first ask how the horizontal salt flux under the camp compares with the expected vertical flux at the lead surface. In steady state the net change in horizontal salt flux beneath the lead should balance the vertical flux at the lead surface. The profile of net change in horizontal flux is given by

$$\bar{q}(z) = \rho[(VS)\text{downstream} - (VS)\text{upstream}]$$

$$\approx \rho \Delta S(z) \bar{V}(z) \quad (1)$$

where ρ is the water density, $S(z)$ is salinity, and $V(z)$ is the horizontal velocity; $\Delta S(z)$ is the change in salinity across the lead. The approximation applies if the mean velocity $\bar{V}(z)$ is much greater than the lead-induced velocity perturbations. If the convection is in steady state, the integral of $\bar{q}(z)$ with depth should equal the salt rejected at the surface across the lead in a strip of unit width parallel to $\bar{V}(z)$. Here we use the velocity measured with the APS to approximate $\bar{V}(z)$. It is necessary to have upstream and downstream profiles of salinity. We assume the measurements were downstream of the lead because the measured salinity increased, but we lack an upstream salinity profile. Therefore a linear curve was fitted to the time records of 1-m depth-averaged salinity values for 24 hours prior to the lead opening. This linear fit was then used to extrapolate an upstream (or undisturbed) salinity profile. This extrapolated profile was subtracted from measured profiles to estimate $\Delta S'(z)$ in (1).

Figure 6 shows $\bar{q}(z)$ averaged over the last hour of data. (The velocity and salinity profiles correspond to those of Figure 4.) The error bars for $\bar{q}(z)$ shown in Figure 6 were calculated using the extrapolated upstream salinity and the standard deviation of the linear curve fit. The salt flux in the mixed layer is significantly greater than the noise level, while below the pycnocline, the salt flux is negligible. At the pycnocline, the negative salt fluxes occur because $\Delta S'(z)$ is negative because of the deepening of the pycnocline. The total salt flux (integral of $\bar{q}(z)$ over z) is 0.55 $g\ cm^{-1}\ s^{-1}$ in a direction toward about 20° true above 50 m. The calculated net horizontal flux integrated over the whole profile should not be affected by mixed layer salinity changes due to entrainment, but should reflect the salt added at the surface. This salt is confined to the mixed layer (top 40 m), so the mixed layer salinity change caused by surface flux alone is the net horizontal flux divided by the average mixed layer velocity of 4.7 cm s^{-1}. This amounts to 0.03 PSU, or two thirds of the observed salinity change; the balance of the observed change is due to redistribution of salt in the water column.

The total vertical salt flux at the lead surface should balance the calculated total horizontal flux. Here the fetch of open water contributing salt to the mixed layer is estimated by dividing the horizontal salt flux in the ocean by the estimated salt flux per unit area at the surface. The required fetch is then compared with the lead geometry. Determining the salt flux at the lead surface involves calculating the rate of ice growth and the salinity of the new ice. The difference between the salinity of the new ice and the water from which it was formed yields the salt rejected at the surface.

Several authors have dealt with the estimation of ice growth rates. *Anderson* [1961] gives an empirical expression for the ice growth rate h based on field measurements:

$$\dot{h} = dh/dt = [B_2(T_w - T_a)]/(2h + B_1) \quad (2)$$

where T_w is the water temperature (assumed to be the freezing temperature), T_a is the air temperature, and h is the ice thickness. B_1 and B_2 are constants equal to 5.1 cm and 7.75 × 10^{-5} $cm^{-1}\ s^{-1}$, respectively. On the basis of a theoretical examination of the heat flux through ice and open water, Maykut (personal communication, 1979) reports

$$\dot{h} = \frac{1}{\rho_i \lambda}\left[-\frac{k_i}{k_i + (C_t + A)h}(C_t\theta + A\theta')\right] \quad (3)$$

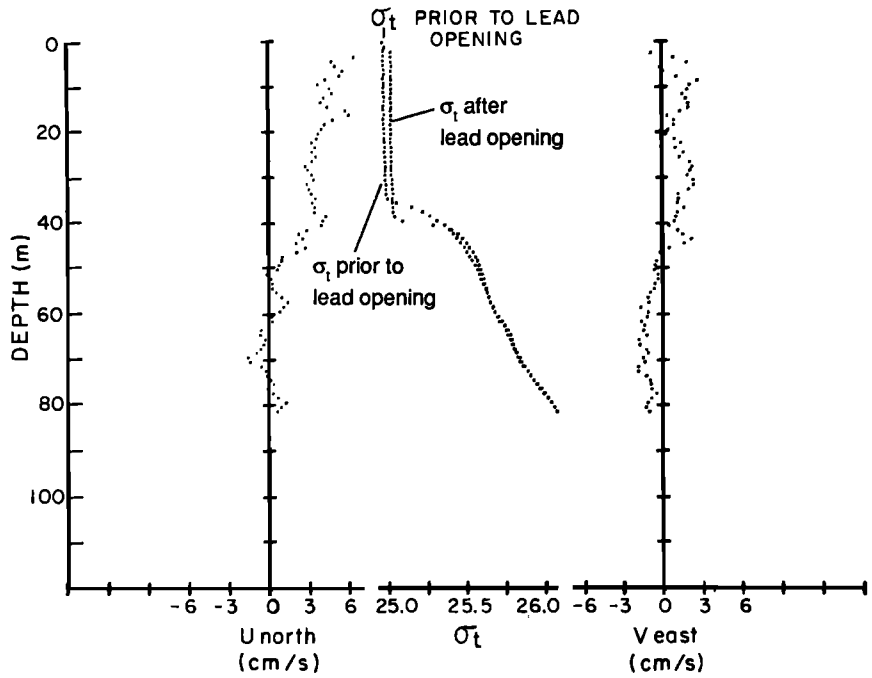

Fig. 4. Velocity and σ_t averaged from 1430 to 1530 AST (after the lead was open) on April 10, 1976, at the AMLE ice camp. Also shown is a σ_t profile measured before the lead opened.

where

k_i conductivity of sea ice, equal to 4.63×10^{-3} cal cm^{-1} s^{-1} $°C^{-1}$;
$A = 8.68 \times 10^{-5}$ cal cm^{-2} s^{-1} $°C^{-1}$;
$C_t = a_1 \rho_a C_p C_e U_a$, equal to $\{1.15 \times 10^{-6}$ (cal cm^{-2} s^{-2})/(cm s^{-1})$\}$ U_a;
U_a wind speed at 2 m, in cm s^{-1};
$\theta = T_a - T_w$;
$\theta' = T_e - T_w$;
$T_e = \varepsilon^{1/4} T_a = (0.7855 + 0.000312\ G_c^{2.75})^{1/4} T_a$;
$G_c = 10 \times$ fraction of cloud cover.

The θ term in (3) accounts for the sensible and latent heat loss, while the θ' term accounts for heat loss caused by long wave radiation. The heat required to produce 1 cm^3 of solid ice, $\rho_i \lambda$, is 72 cal cm^{-3}. When predicting the growth rate of a porous ice sheet, Maykut uses $\rho_i \lambda$ equal to 55 cal cm^{-3}.

Converting these ice growth rates to salt flux requires an estimate of how much salt is rejected from the ice as it

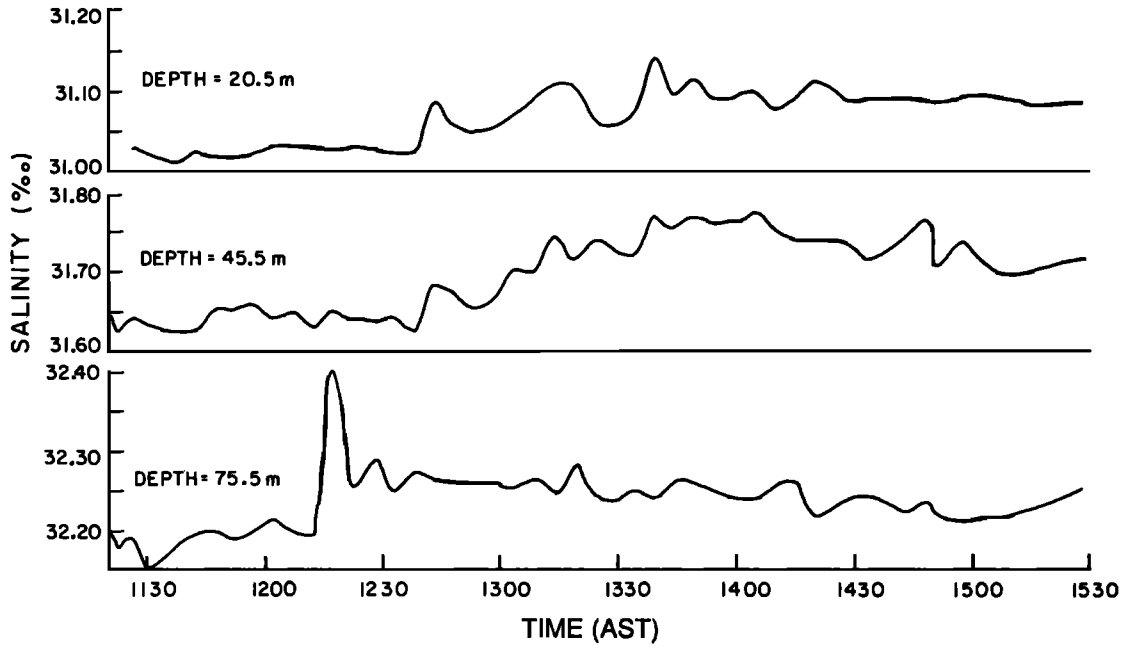

Fig. 5. Salinity versus time at 20.5, 45.5, and 75.5 m at the AMLE ice camp on April 10, 1976. The lead opened about 1200 AST.

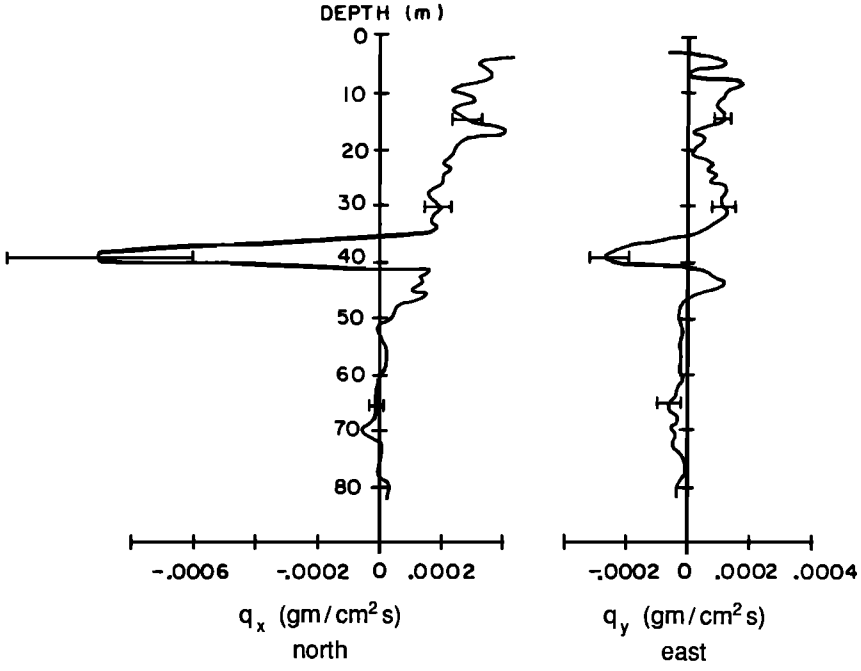

Fig. 6. The salt flux, $\bar{q}(z) = \rho\,[S_{\text{downstream}} - S_{\text{upstream}}]\bar{V}$, averaged over the last hour of data. (The velocity and measured salinity profile correspond to those of Figure 3.) The error bars shown for $q(z)$ were calculated using the extrapolated upstream salinity and the standard deviation of the linear curve fit.

grows. Based on laboratory experiments, *Cox and Weeks* [1975, 1988] indicate the surface salt flux can be expressed as

$$F_s = \rho_i \dot{h}[1 - k_c]S_w \tag{4}$$

where S_w is the water salinity fraction, ρ_i is the ice density (0.9 g cm^{-3}), and

$$k_c = 0.8439 + 0.0529 \ln \dot{h} \qquad \dot{h} < 2 \times 10^{-5} \text{ cm s}^{-1}$$

$$k_c = 0.26[0.26 + 0.74e^{-7234\dot{h}}]^{-1} \qquad \dot{h} > 2 \times 10^{-5} \text{ cm s}^{-1}$$

However, there is some uncertainty about the appropriate values of k_c. *Cox and Weeks* [1975, 1988] obtained their data for high growth rates using a laboratory setup with a very low salinity. The resulting values of k_c for high growth rates are probably too high for field conditions (J. Wettlaufer, personal communication, 1991). Judging from salinity samples of new ice, the maximum value of k_c is about 0.5, so in our subsequent calculations, k_c is never allowed to exceed this value. Also, the formulas for k_c are only appropriate when the ice is of finite thickness. In fact, the surface of a lead is often ice free because wind stress moves surface water and ice crystals to the downwind edge of the lead [*Pease*, 1980; *Bauer and Martin*, 1983]. If the newly formed ice crystals are swept downstream under the pack ice, the salinity of new ice may be effectively zero and k_c equal to zero. However, wind-swept new ice is often often observed to collect at the downwind edge in a wedge with a salinity of 10–15 per mil. If no ice escapes from the wedge, k_c for the lead taken as a whole may then be 0.3–0.5.

At the time of lead opening in the AMLE the water temperature was −1.8°C, the air temperature was −16.8°C, and S_w was 31 PSU. The average 2-m wind speed was 4.5 m s^{-1}, and cloud cover was about 60%. For these conditions and k_c equal to zero, the open water salt flux is 6.4×10^{-6} g cm^{-2} s^{-1}, using Anderson's formulation (equation (2)) and 30% less, 4.6×10^{-6} g cm^{-2} s^{-1}, using Maykut's equation (3). Anderson's equation is based on field data. Because it is difficult to measure growth rates in open water, his formula may be an extrapolation from data for finite thickness. Maykut's equation (3) is based on a complete theoretical analysis of the thermodynamic exchanges at the lead surface and includes the effect of long wave radiation. It agrees well with his more sophisticated theoretical model [*Maykut*, 1978].

The open water fetch over which these fluxes would have to act to produce a 0.55 g s^{-1} total salt flux is 865 m for *Anderson* [1961] and 1205 m for Maykut (personal communication, 1979). For k_c equal to the upper limit of 0.5, the salt flux figures would be halved, and the required fetch figures would be doubled. In short, to produce the observed total salt flux, a fetch of about 1–2 km is required. This is much greater than the estimated lead width of approximately 100 m at 1500 AST on April 10. However, it is possible to achieve large open water fetch if the relative flow direction under the lead is at a small angle to the lead axis (a relative angle of 3° produces a fetch of 2 km for a 100-m lead). The large fetch is not unreasonable, at least given our crude estimates of the lead and flow geometry.

Going beyond the steady state view, another question concerns how the observed salinity disturbance could have developed in such a short time. The predicted salt fluxes would require 5–7 hours (10–14 hours for $k_c = 0.5$) to raise the mixed layer salinity 0.03 PSU. Yet the salinity increased much more rapidly than this after the lead opened next to the AMLE camp. The rapid salinity rise may suggest salt was added to the mixed layer starting several hours earlier a few kilometers away from the camp and then was advected past. In fact, the photographs on which Figure 3 was based indicate the opening of the lead was due in part to a differential rotation, between the camp floe and the floe to

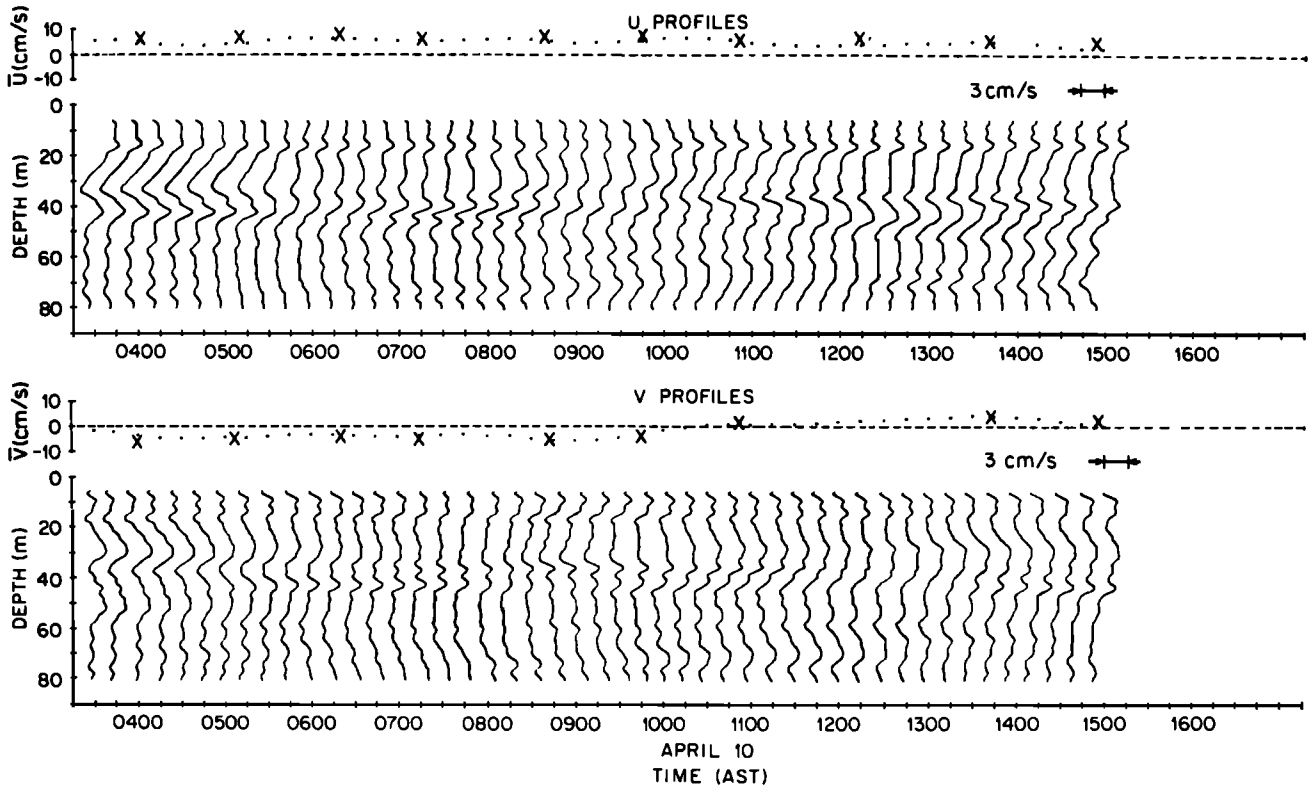

Fig. 7. Velocity profiles measured with the APS at the AMLE ice camp from 0330 to 1500 AST on April 10, 1976. Positive current jets in u (toward open water) at 15 m, and negative jets (away from open water) at 38 m appear from around 1100–1430 AST.

the west, about a point north of the camp. If this pivoting was part of the initial motion, the lead 2–3 km south of the camp may have achieved significant width several hours earlier than the lead by the camp. Another possible factor in the rapid salinity rise might be small scale spatial and temporal variability in the convection process. Recent modeling studies [*Fernando et al.*, 1991; also D. C. Smith IV, personal communication, 1991] indicate convection may occur in periodic concentrated pulses. Such episodic convection serves to concentrate the salinity disturbances in time and space, so the observations at a single point and over a short period of time, as at AMLE, may not give a good average description of the phenomenon.

The simple salt balance calculations indicate lead convection can account for the observed response if the flow was nearly along the axis of the lead, which appears to be true, and the lead opened earlier to the south, which is possible. *Estoque and Bhumralkar* [1969] examine the case of buoyant convection in the atmosphere when the mean flow is along the axis of a source, using a numerical model of flow over a two-dimensional heat island. This resembles the AMLE case. In their results the convective cells are active perpendicular to the sides of the source, but the disturbance in the mass field is not spread away from the source by the mean flow.

The shape of the AMLE lead is far from simple, but the velocity data suggest a possible cellular circulation on a very localized scale even though the lead was not straight. Although there were no large changes in the velocity structure, a weak but significant jet did appear in the mixed layer when the lead opened. Jets are especially apparent in the u velocity profiles made around 1400 AST, shown in Figure 7. At 15 m depth there is a 2 cm s^{-1} jet to the north, perpendicular to the lead where it was closest to the measuring site. It persists from 1100 AST to the end of the experiment and is also shown in Figure 4. Figure 7 also displays a jet in u at 38 m depth which persists from 1100 to 1430 AST. Its magnitude is about 2 cm s^{-1} and it is directed south, away from the lead. This pattern is consistent with cellular convection; the jet at 38 m may be driven by the descending brine plume in the lead immediately to the north of the camp, and the jet at 15 m may supply an influx of mixed layer water to the lead surface. The density disturbances associated with these jets would most likely be obscured by the dominant salt flux along the lead axis.

Perhaps a more likely explanation for the jets is that they represent a geostrophic adjustment to the salinity disturbance in the lead. Preliminary numerical model results of D. C. Smith IV (personal communication, 1991) suggest that a cyclonic flow (parallel to the lead, with the lead on the left) develops near the surface next to a freezing lead and an anticyclonic flow develops at the base of the mixed layer. This buildup progresses over several hours as the salinity disturbance builds up. The thermal wind equation suggests a 4 cm s^{-1} shear over 23 m and corresponds to a horizontal salinity gradient of 0.05 PSU over about 2.5 km. Thus the scales of the lead geometry, the salinity disturbance, and the velocity jets are consistent with geostrophic adjustment along the large-scale axis of the lead. Their appearance when the lead opened at the camp would only be consistent with the notion that the observed response is not local to the camp but is due to larger-scale effects which began earlier.

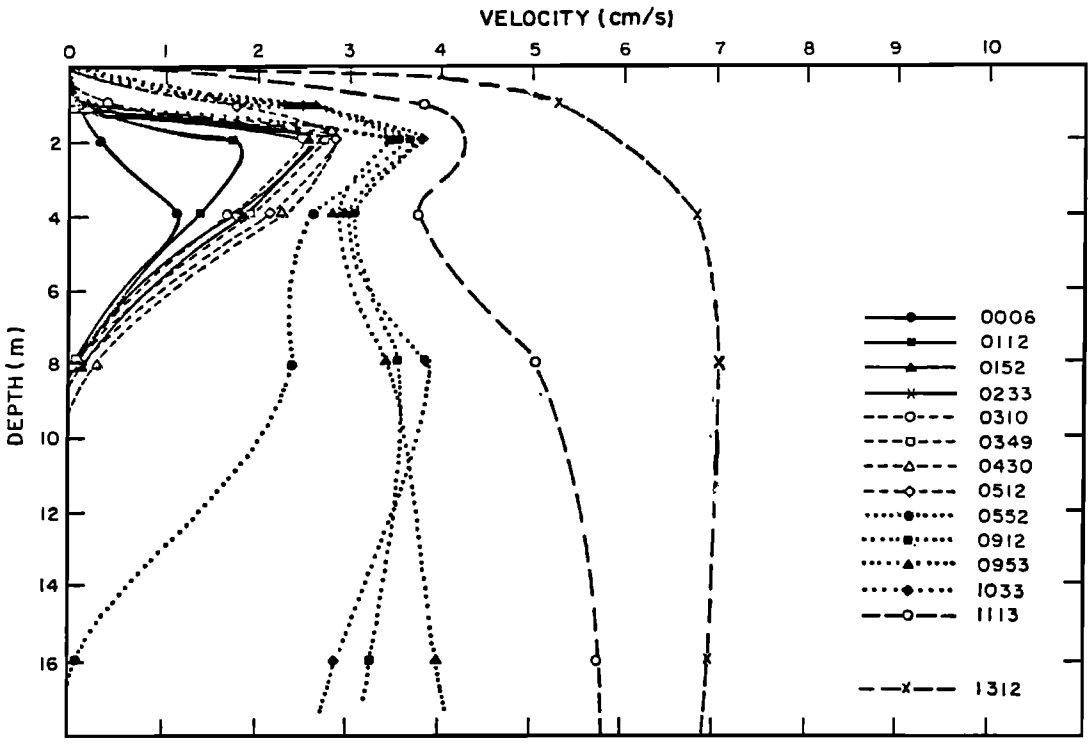

Fig. 8. Current speed profiles before and at the beginning of a storm in early April 1971. Note the jet centered between 2 and 4 m below the ice prior to the increase in ice velocity that resulted in stronger relative flow. The jet is thought to be related to freezing in a lead. The air temperature at the time was −29°C.

Other Measurements of Lead Convection

Some of the best examples of lead convection come from velocity measurements made in the mixed layer during very calm conditions when the relative currents are otherwise nil. The first indication that a circulation pattern like that shown in Figure 1 might be associated with leads came from analyzing velocity records from the 1971 AIDJEX pilot study in the Beaufort Sea [*Smith*, 1973]. Figure 8 shows a series of current speed profiles made at the beginning of a storm. The profiles are from five-point measurements obtained with three-component current meter "triplets" mounted on tubular masts suspended from the ice (an arrangement similar to that used in the AMLE). The feature of interest is the jet extending from the surface to 8 m depth. The jet was observed prior to 0512 AST when the ice velocity and relative water velocity below 8 m was zero. Clearly, some sort of near-surface pressure gradient had to be causing this jet. *Smith* [1973] maintains that such a highly baroclinic feature could not persist for as long as it did, approximately 4 hours, in the homogeneous fluid just beneath the ice were it not for local convection patterns caused by lead circulation. After 0512 AST a storm began, the ice began to move, and the velocity profile displayed the boundary layer type character shown in the later profiles. Although the jet could not be associated with a particular lead, *Smith* [1973] hypothesizes that leads were likely to have been forming just prior to the storm.

A similar surface jet was observed during the fourth ice deployment of ALEX (ALEX4). Figure 9, from *Smith* [1974] and *Smith et al.* [1990], shows a combined density profile and current speed plot made during that experiment. In ALEX4 a camp was established for 3 days at the edge of a lead 52 km, 18° true from Barrow, Alaska. The lead was covered with 10 cm of ice with scattered areas of open water. The jet is illustrated in Figure 9 which shows a typical density profile and successive 40-min averages of current speed starting at 1730 AST on April 3, 1974. The jet was directed toward a group of open water areas 200 m from camp and toward two open leads 1 km beyond the lead by which the camp was established. As discussed by *Smith* [1974], the jet was a persistent feature with a velocity maximum only 0.5 m beneath the ice. Outside the jet the currents were generally below 1 cm s^{-1}. The maximum velocity in the jet ranged from 3 to 12 cm s^{-1}; the high values occurred in the late evening when the wind speed increased and the low values occurred at midday when the wind speed was lower. The differences may have been due to differences in heat flux over the open water. The close proximity of this jet to the surface, the direction of the flow, and its fluctuation in intensity with freezing rate suggest that it was part of the lead convection pattern.

The two cases discussed above are examples of surface jets supplying freshwater inflow at the surface of leads. A jet that may have been associated with lead convection has also been observed at the bottom of the mixed layer. During the third ice deployment of ALEX (ALEX3) such a jet was observed deep in the mixed layer. In this experiment a camp was established on multiyear ice 44 km, 23° true from Barrow, Alaska. Figure 10 shows the jet as measured with fixed current meters in two successive 40-min. averages starting at 0540 AST on April 9, 1974 along with a density (σ_t) profile typical of ALEX3 conditions. The argument relating a jet deep in the mixed layer to lead convection cannot be as strong as for surface jets because of the

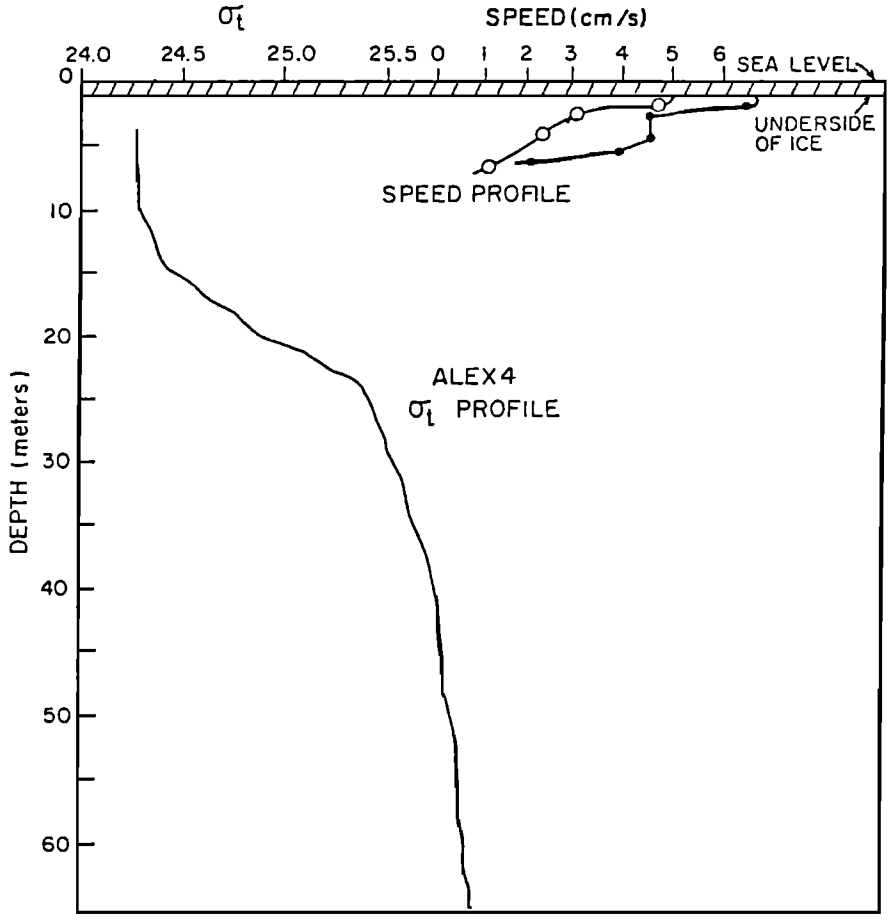

Fig. 9. Velocity and σ_t profiles from ALEX4. Air temperature at the time was −25°C.

possibility of small-scale baroclinic currents in the stratified region at the top of the pycnocline, but the character of the jet and the circumstances suggest a possible connection with lead convection. As described by *Smith* [1974], the jet persisted through the three-day deployment, the maximum speed ranging from 5 to 8 cm s^{-1} and the depth decreasing from 15 to 12 m. The top of the pycnocline was at 15 m. During ALEX3 there were no active leads nearby, but the direction of flow in the jet was offshore away from a large (2 km across) active shore lead.

Density data gathered during the second ALEX deployment (ALEX2) show evidence of penetrative convection. The density profiles shown in Figure 11 were gathered during ALEX2. On this occasion, two camps were established on either side of a lead 33 km, 5° true from Barrow. The lead was oriented east-west, and the wind was blowing toward the south. This would have been an ideal site for comparing the density and velocity structure upstream and downstream of a lead. Unfortunately, the camps drifted apart laterally, the lead closed and formed a pressure ridge at the upstream camp, and that had to be evacuated. The lead remained open at the downstream camp, and evacuation was delayed there for 24 hours. During this time the profiles of Figure 11 were obtained 50 m from the edge of the open lead. The relevant aspect of these plots is the degree of variability shown at the pycnocline. During the period 2204–0039 AST, masses of low-density (hence low-salinity) water penetrated to as deep as 25 m, even though the pycnocline was at a depth from 10 to 15 m. The intrusions were short-lived and often caused unstable stratification. The profiles bear a strong resemblance to the single thermocouple, temperature profile in the laboratory study of penetrative convection by *Deardorff et al.* [1969]. The profiles suggest dense plumes from the surface were entraining less dense water from the mixed layer and penetrating the pycnocline. The profile at 2305 AST shows the greatest penetration depth, 25 m. During relatively quiet periods, the density (salinity) at 25 m exceeded that in the mixed layer by 0.25 σ_t units. Therefore the penetration to 25 m implies portions of the plume must have had a peak density at least 0.25 σ_t units greater than the surrounding surface water. Typical perturbations in the profiles are 0.05 σ_t units (0.06 PSU), which suggests the average perturbations in salinity as a result of lead convection were of this order. Because of the shallow depth of the mixed layer, the salt rejected at the lead surface was confined to a shallow region and the resultant salinity disturbance is relatively large. Also, the wind and currents were calm when the measurements were made, so the salt rejected at the surface was not spread out horizontally.

Another prominent feature of Figure 11 is the mixed layer at the bottom of the profiles. The water depth at the site was about 115 m. The deepest 10–20 m of the water column was 0.015 σ_t units greater in density than the bulk of the water column. As reported by *Smith* [1974], the water temperatures throughout the water column at ALEX2 were very close (within 5 millidegrees) to the freezing point. (Indeed,

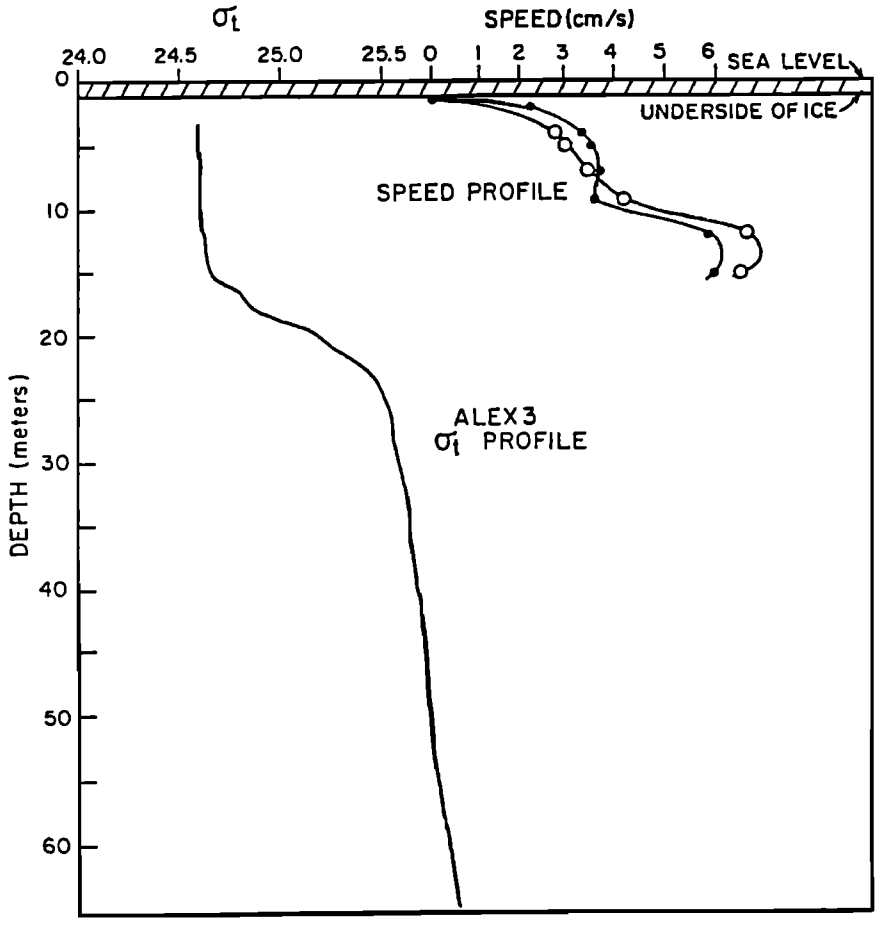

Fig. 10. Velocity and σ_t profiles from ALEX3. Air temperature at the time was −23°C. The two velocity profiles represent successive 40-min averages beginning at 1747 AST on April 3, 1974 [from *Smith*, 1974].

this was true for the most part at all the ALEX sites.) Thus the high salinity layer had a surface freezing origin, and it may have been due to convection in the large open-shore lead.

A final example illustrates once more how complex (and difficult to interpret) lead processes can be. In March and April of 1987 an ice camp designated the Prudhoe Bay Experiment (PRUDEX) was established about 185 km north of Prudhoe Bay, Alaska. As part of the experiment, three turbulence clusters, employing triads of Smith velocity sensors and Sea-Bird temperature and conductivity probes, were deployed at 2, 4, and 5 m below the ice. On day 88 (March 29) a lead opened at the west edge of the camp. The location of the lead relative to the camp is illustrated in Figure 12, a sketch based on an airborne observation done on day 89 (March 30). The lead pattern obviously was not an idealized one; the lead ran north-south with a loop around the camp. There were also other leads and areas of thin ice near the camp in every quadrant. The camp was on the upwind side of the main lead.

Figure 13 shows the wind velocity, ice velocity, absolute currents, salinity, temperature, and turbulent intensity from day 88.5 (midday, March 29) to day 90.5 (midday, March 31). After the lead first opened at 88.75, the ice drift and currents were as one would expect for purely wind-driven motion. The ice velocity was about 2% of the wind speed and a few degrees to the right. The currents were slightly lower and more to the right. The salinity remained at about 30.01 PSU. Ten hours later, at day 89.2 the salinity rapidly dropped 0.06 PSU and the 2- and 5-m currents veered to the right from the purely wind-driven motion. This indicates the camp moved over a relatively fresh patch of water downstream of the lead, not something one would expect given our notion of lead convection. Subsequently, the salinity rose and the currents returned to a pattern consistent with wind forcing. Then, from day 89.8 to 90.5 the currents at 2 and 5 m were larger than the ice velocity and toward the lead. This was not wind-driven, and we suspect it is part of the lead convection pattern. It is not clear why it took over 24 hours to start, but this may be related to the time required to spin up the convection pattern. The turbulent intensity decreased as the front passed at 89.2 and again when the anomalous currents started late on day 89. This is conceivably due to local increases in stratification. It is difficult to provide a simple explanation of these observations. Aside from the initial salinity drop, they are consistent with a gradual spin-up of lead convection, with a rising salinity downstream and at least short periods of inflow in the near surface water. Much of the complication may be due to the effects of other nearby leads. Indeed, in such active areas it may always be difficult to examine the effect of a single lead.

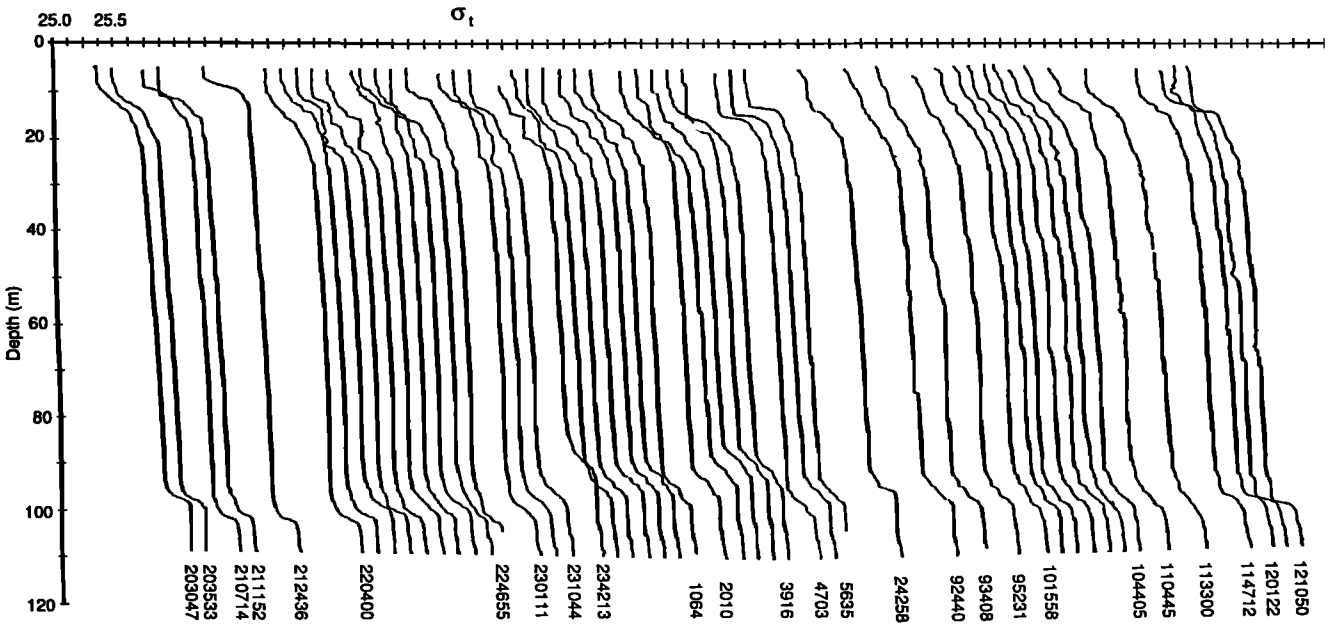

Fig. 11. Successive σ_t profiles from ALEX2 showing fluctuations indicative of brine plumes penetrating the pycnocline. The horizontal scale is 0.125 σ_t units per division. Casts were made in groups with about 4.77 min between casts. Successive cast profiles are separated by one σ_t division. Groups of profiles are separated by two or three divisions. The time, on March 25–26, 1974, of the first and last profile in each group is indicated. The air temperature was about −28°C.

3. Scales of Lead Convection

The observations discussed above provide glimpses of several forms of lead convection. The velocity observations from the AIDJEX pilot study, ALEX, and AMLE are indicative of free convection in which the density disturbances resulting from salt flux cause pressure gradients which in turn drive a cellular convection pattern like that shown in Figure 1. The density observations from ALEX2 show penetrative convection. All these observations were made when there was very little ice motion, and so we might expect these types of convection. We would expect a forced type of convection when the ice velocity is high. Then there is sufficient turbulence in the mixed layer to mix the injected salt uniformly through the mixed layer, preventing pressure gradients and the cellular circulation patterns from developing. Depending on how high the ice velocity has to be to cause forced convection, it may be more common than free convection. The salinity data from AMLE may be an example of forced convection. In general, forced convection will not show up as readily in hydrographic and velocity data because the salinity disturbance is spread over a relatively large area and depth range.

Scaling arguments can be used to predict how great the ice velocity must be to cause forced convection. They can also be used to estimate the magnitude of the velocity and density disturbances in the case of free convection. In what follows, the lead axis is taken perpendicular to the ice velocity, and the wind stress on the water is assumed to scale with the underice stress. We assume that the coordinate system, moving with the ice, is as shown in Figure 1 and that y derivatives are zero. The flow is assumed to be hydrostatic. This may not be strictly applicable for a case with absolutely no ice velocity and hence no mean advection of salt, but it should be suitable for velocities anywhere near those where forced convection is a consideration. The equations of motion are

$$\frac{\partial u}{\partial t} + u\frac{\partial u}{\partial x} + w\frac{\partial u}{\partial z} + fv = \frac{-1}{\rho_o}\frac{\partial p}{\partial x} + \frac{\partial}{\partial z}\left[K\frac{\partial u}{\partial z}\right] \quad (5)$$

$$\frac{\partial v}{\partial t} + u\frac{\partial v}{\partial x} + w\frac{\partial v}{\partial z} - fu = \frac{\partial}{\partial z}\left[K\frac{\partial v}{\partial z}\right] \quad (6)$$

$$\partial p/\partial z = g\rho = gMs \quad (7)$$

$$\partial(\rho u)/\partial x + \partial(\rho w)/\partial z = 0 \quad (8)$$

$$F_s L_L = \int_0^\infty [\langle us\rangle_{x=L_L} - (us)_{x=0}]\, dz \quad (9)$$

$$\frac{\partial s}{\partial t} + u\frac{\partial s}{\partial x} + w\frac{\partial s}{\partial z} = \frac{\partial}{\partial z}\left[K\frac{\partial s}{\partial z}\right] \quad (10)$$

where u, v, and w are velocities in the x, y, and z directions, ρ is the perturbation density, p is the perturbation pressure, f is the Coriolis parameter, K is the eddy coefficient, M is $\partial\rho/\partial s$, s is the perturbation salinity, and F_s is the salt flux at the lead surface. Denoting nondimensional variables with a tilde (~), the following scaling is applied:

$$u = U_i\tilde{u}$$

$$v = U_i\tilde{v}$$

$$x = L_L\tilde{x}$$

$$z = d_s\tilde{z}$$

d = mixed layer depth

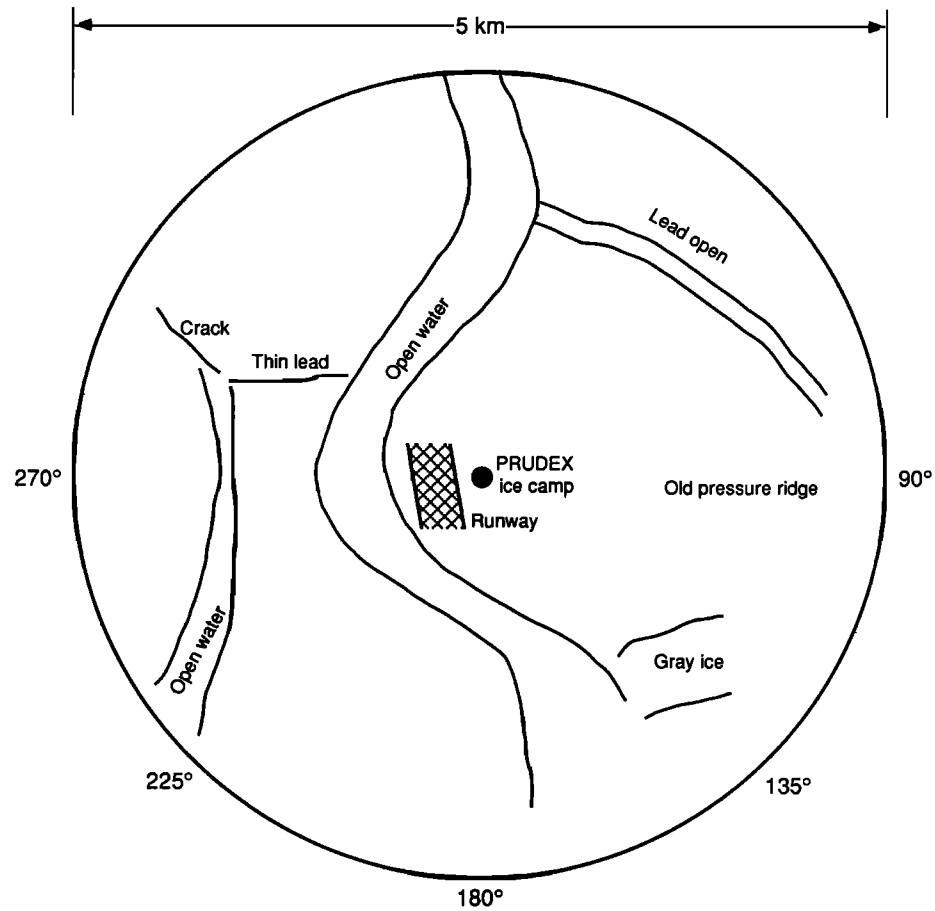

Fig. 12. A sketch of the PRUDEX ice camp area based on an airborne observation done on March 30, 1987. It shows the lead that opened around the camp on March 29. The lead pattern obviously was not an idealized one; it ran north-south with a loop around the camp. There were also other leads and areas of thin ice near the camp in every quadrant. The camp was on the upwind side of the main lead.

$$K\frac{\partial u}{\partial z} = \frac{\bar{K}u_i}{d}\frac{\partial \tilde{u}}{\partial \tilde{z}} = u_*^2 k_d \frac{\partial u}{\partial z}$$

$$t = T\tilde{t}$$

$$w = W\tilde{w}$$

$$p = \Pi\tilde{\rho}$$

and

$$s = \Delta S\tilde{s}$$

where u_* is the friction velocity, $(\tau_{z=o}/\rho_o)^{1/2}$, and T, W, Π, and ΔS are scales to be determined. Applying this scaling to (8) yields

$$W = U_i d/L_L \tag{11}$$

Scaling (9),

$$\Delta S = F_s L_L/U_i d \tag{12}$$

Using this relation, scaling (7) gives

$$\Pi = gMF_s L_L/U_i \tag{13}$$

Using these scales to obtain a nondimensional version of the cross-lead momentum equation gives

$$\frac{L_L}{U_i T}\left[\frac{\partial \tilde{u}}{\partial \tilde{t}}\right] + \left[\tilde{u}\frac{\partial \tilde{u}}{\partial \tilde{x}} + \tilde{w}\frac{\partial \tilde{u}}{\partial \tilde{z}}\right] + \frac{fL_L}{U_i}[\tilde{v}] = -\frac{gMF_s L_L}{U_i^3 \rho_o}\left[\frac{\partial \tilde{p}}{\partial \tilde{x}}\right] + \frac{u_*^2 L_L}{dU_i^2}\left\{\frac{\partial}{\partial \tilde{z}}\left[k_d \frac{\partial \tilde{u}}{\partial \tilde{z}}\right]\right\} \tag{14}$$

In the case of free convection, the pressure gradient dominates the right-hand side of (14); for forced convection, the turbulent stress term dominates. The ratio of the two terms is

$$L_o = gMF_s d/\rho_o U_i u_*^2 \tag{15}$$

This is the vertical scale d divided by a type of Obukhov length. When the turbulent stress gradient is of the same order as the buoyancy flux-induced pressure gradients in the mean momentum balance, the lead number is of the order of 1. Substituting $u_*^2 = C_d U_i^2$ yields

$$L_o = gMF_s d/\rho_o C_d U_i^3 \tag{16}$$

For the parameterizations used here for the lead problem, L_o will be called the lead number. Using (3) and (4) to calculate F_s and taking $C_d = 0.0055$ and $M = 0.793$, (16) has been used to calculate ΔT versus U_i for $L_o = 1$. The results for various values of h are plotted in Figure 14 for d

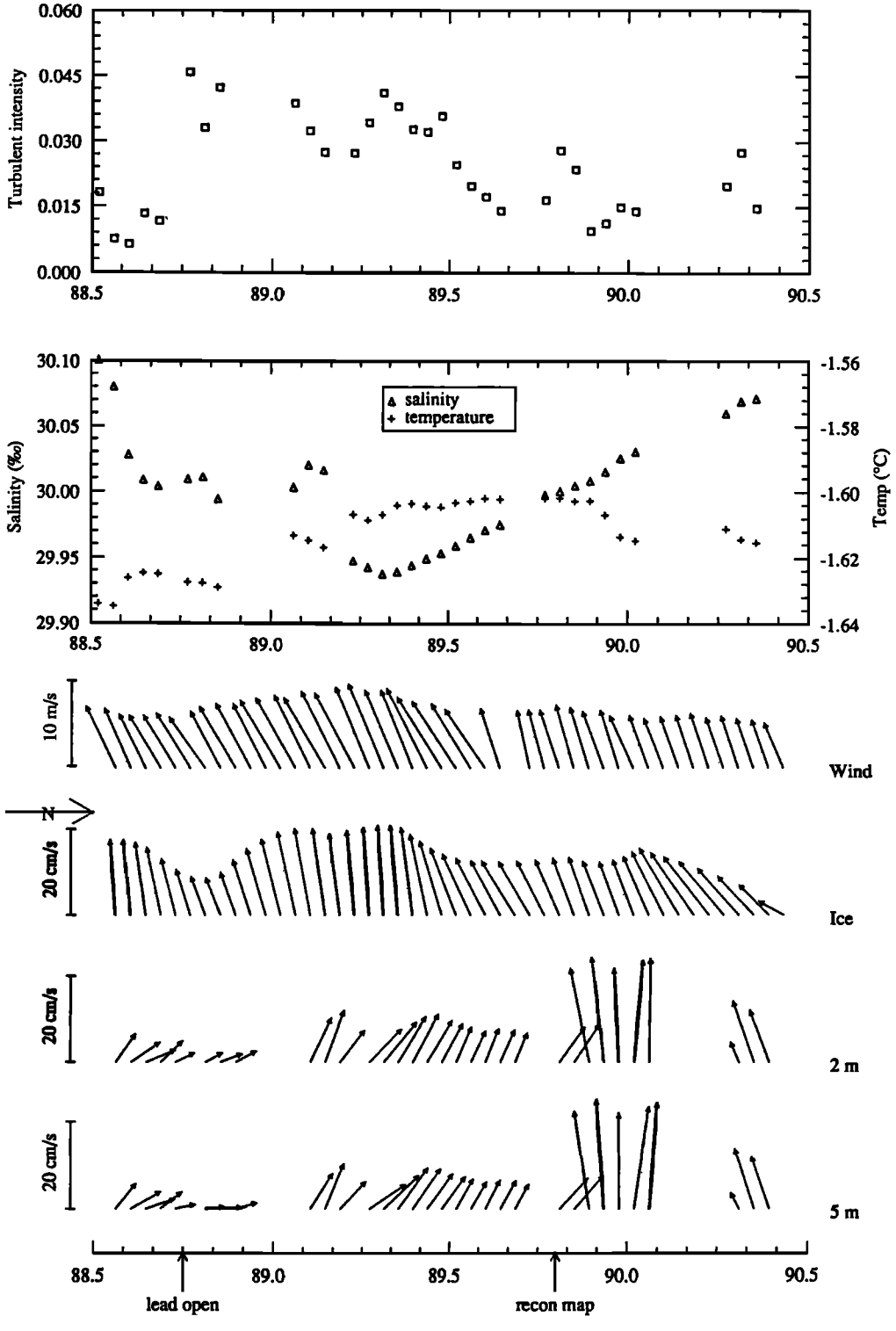

Fig. 13. The wind velocity, ice velocity, absolute currents, 5-m salinity, temperature, and turbulent intensity from day 88.5 (midday, March 29) to day 90.5 (midday, March 31) of 1987 at the PRUDEX ice camp. The lead first opened at 88.75. Aside from the initial salinity drop, the measurements are consistent with a gradual spin-up of lead convection, with a rising salinity downstream and at least short periods of inflow in the near surface water.

equal 35 m. The formulas for k_c from *Cox and Weeks* [1975, 1988] have been used, but for the reasons described previously, a maximum limit of $k_c = 0.5$ has also been applied. This limit results in the slight slope discontinuity in the curves at high freezing rates. Points above the critical curves correspond to cases in which large-scale convection is driven by the pressure gradients set up by the buoyancy flux. The points below the curves correspond to cases in which the buoyancy flux is simply mixed into the water column by turbulence generated by the ice motion.

A similar nondimensional parameter can be derived by considering the turbulent kinetic energy equation. The ratio

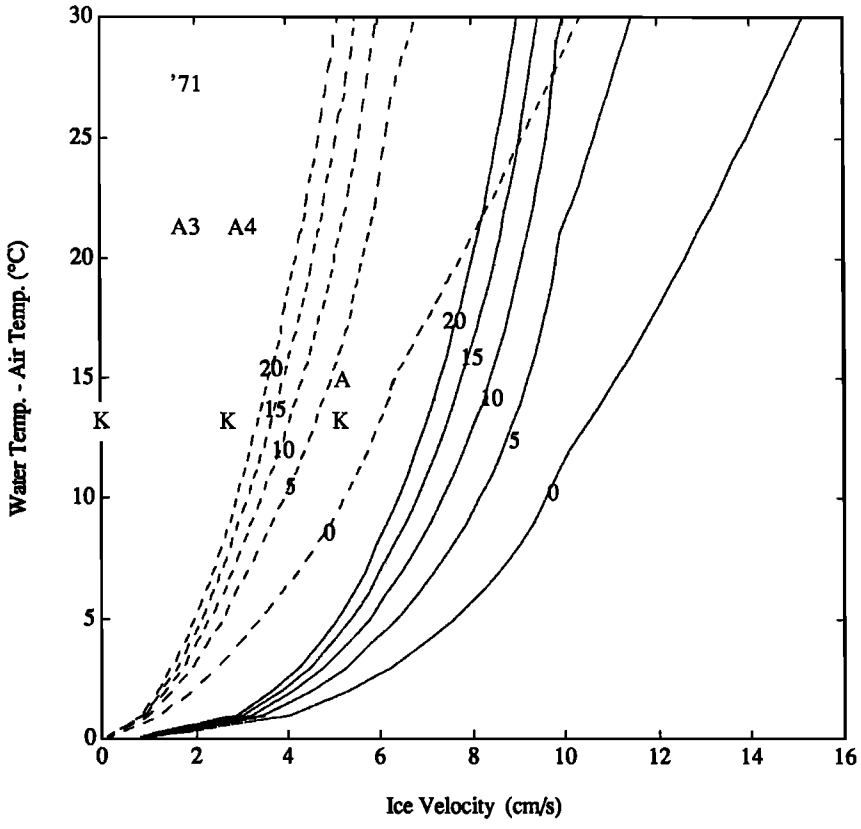

Fig. 14. Air-water temperature difference versus U_i for L_o (solid line) and L_{ot} (dashed line) equal to 1 for various ice thicknesses in centimeters. Also shown are the temperature difference and ice velocity values for various experiments or theoretical examples; '71 denotes the AIDJEX pilot study, A3 denotes ALEX3, A4 denotes ALEX4, A denotes AMLE, and K denotes *Kozo* [1983].

of the maximum, neutral stratification eddy size to the Obukhov length is

$$L_{ot} = (0.05u_*/f)/(u_*^3/kF_B) = \frac{0.05kgMF_s}{fu_*^2\rho_w} \qquad (17)$$

where k is von Karman's constant (0.4) and F_B is the buoyancy flux. This corresponds to the stability parameter of *Tennekes* [1970] put in the context of marine haline convection. The main, effective difference between L_o and L_{ot} is that for L_o, the Obukhov length is compared with a fixed scale of ambient stratification, while for L_{ot}, the Obukhov length is compared with a variable vertical scale proportional to u_* and is not dependent on the ambient stratification. The values of ΔT and U_i for which L_{ot} ratio is 1 are plotted for various ice thicknesses in Figure 14. They have been calculated using the approximations described above. The curves are similar to those for $L_o = 1$, although the critical temperature difference for a given velocity is slightly greater. Thus there are three regimes to consider. For L_o and L_{ot} less than one (lower right in Figure 14), both the large-scale circulation and the turbulence can be described as forced by surface stress. The mean pressure gradients are small compared with mean shear stress divergence in the mean momentum equation, and the buoyant production of turbulence is small compared with shear production. At the other extreme, for L_o and L_{ot} greater than one (upper left), both the large-scale circulation and the turbulence are forced by the buoyancy flux. The mean pressure gradients caused by the average density disturbance are large compared with shear stress divergence, and buoyant production of turbulence is greater than shear production. There is an intermediate range where L_o is greater than 1 but L_{ot} is smaller than one. In this case, shear production may dominate buoyant production in the boundary layer, but the mean pressure gradients caused by the large-scale density disturbance are important in the mean momentum balance.

The ΔT and U_i coordinates for the observations discussed previously (with the exception of ALEX2 for which U_i is unknown) are also shown in Figure 14. The ice velocity in the Arctic is less than 10 cm s^{-1} a great deal of the time, and temperature differences of 15°C or more are quite common. Therefore Figure 14 suggests convection from open leads may often be dominated by buoyancy effects and involve cellular velocity patterns. With the exception of the AMLE experiment, the observations were made when the air temperature was less than −16.8°C and the ice velocity was less than the useful threshold of fixed current meters (2 cm s^{-1}), placing the observations well within the free convection zone. This agrees with the fact that the observations displayed the jetlike structures characteristic of free convection. The AMLE observations yield the smallest lead number, 18, while the other observations, assuming $h = 0$ and wind speeds of 4.5 m s^{-1}, yield lead numbers more than 331. Thus all the observations were made under conditions conducive to free convection.

To define the critical lead number more accurately, data representative of the forced convection regime must be obtained. *Topham et al.* [1983] have described a site near Dundas Island, Canada, where tidal currents of 200 cm s^{-1} keep a polynya ice free year around. A point describing such a site would clearly be in the free convection region of Figure 14. In fact, the turbulent boundary layer at the Dundas Island polynya not only entrains dense brine but buoyant ice crystals as well. Unfortunately, such an extreme site, with lead number of the order of 10^{-4}, is not useful in making a refined estimate of the critical lead number. The observations implying the presence of free convection are relatively easy to recognize because they involve strong perturbations in a relatively quiet density and velocity field. Making observations of marginally forced convection conditions will require a conscious effort to seek out and examine such cases because forced convection involves a small perturbation on a strong boundary layer flow.

In deriving the lead number, the velocity perturbations were scaled with the ice velocity. For forced convection this scaling is appropriate because the flow pattern is that of a turbulent boundary layer and the velocity perturbation varies from the ice velocity at the surface to zero at the bottom of the boundary layer. The observations from the 1971 AIDJEX pilot study, ALEX3, and ALEX4 suggest that when free convection occurs, the maximum perturbations are somewhat greater than the ice velocity. Figures 7–9 illustrate this. However, as a result of the restricted depth range of these disturbances, the velocity averaged over the mixed layer depth is of the same order as the ice velocity. In general, it appears that the convectively driven perturbations near leads are significant for either free or forced convection.

Leads can have longer-term, larger-scale effects on the velocity field. Leads are usually open and active for at least a day. The resulting density disturbance might be expected to set up a geostrophic flow and persist in some form for days after the lead closes. This presumes that the initial buoyancy-driven disturbances are significant within an inertial time scale. The time scale for the development of the cross-lead velocity disturbance is given by comparing the time derivative term in (14) with the buoyancy term

$$T_u = \rho_o U_i^2 / gMF_s \tag{18}$$

Because the density disturbance varies only in the cross-lead direction, T_u is also the time scale for the development of the density perturbations. Taking conditions from the AMLE experiment as a typical example (U_i = 5 cm s^{-1}, ΔT = 15 °C), T_u is found to be approximately 2.2 h. This is of the order of the time required for surface freezing to fill the mixed layer with enough salt to bring the salinity to the equilibrium value. Thus the cross lead velocity and density disturbance can develop on a time scale of the order of the inertial time scale. Also, for time scales longer than the inertial time scale, the acceleration term in (14) will be smaller than the Coriolis term.

Balancing the Coriolis term against the pressure gradient term yields a velocity scale, V_g, for the geostrophic secondary flow. Using L_L as the horizontal length scale and Π (from (13)) as the pressure scale yields

$$V_g = gMF_s / fU_i \rho_o \tag{19}$$

For the AMLE conditions V_g is 3 cm s^{-1}, or of the same order as U_i. This is not because u was initially assumed to scale with U_i because the Coriolis term was not used in deriving the pressure scaling. It can be argued that the pressure gradient used in (19) is a maximum and should only apply close to the lead. For distances far from the lead a more appropriate length scale might be the distance traveled by the lead in an inertial period U_i ($2\pi/f$). This scale is also of the order of the distance traveled during the active life of the lead and therefore of the order of the space occupied by the density disturbance. For the AMLE data this distance is 3 km. Assuming the maximum pressure can be scaled as in (14) and using a horizontal length scale of 3 km yields a V_g of 0.5 cm s^{-1}. In the near field the geostrophic velocity scale is significant for typical conditions; in the far field it is small but significant.

For very low ice velocities near zero (pure free convection) the appropriate velocity scale to be applied on the right side of (18) and (19) should probably be limited to being no smaller than the velocity scale of free convection. As will be discussed below, modeling studies of this regime suggest this scale is typically about 1 cm s^{-1}. For such a case the time scale would be a maximum of a couple of days, and the geostrophic velocity might be as great as 15 cm s^{-1}. It is unlikely that the ice velocity would remain zero or that the lead would remain open for this length of time in pack ice conditions. However, such a situation might arise in specialized situations such as semipermanent shore leads or other shorefast ice conditions.

In considering the effects of leads on the density field, recall that the observed lead-induced salinity perturbation during the AMLE was 0.03 PSU (0.024×10^{-3} g cm^{-3} density fluctuation). The maximum observed salinity fluctuations directly under a lead were 0.3 PSU as inferred from the ALEX2 data. In general, the lead-induced salinity perturbations are a small but significant fraction of the annual variation in mixed layer salinity, 0.36 PSU (0.29×10^{-3} g cm^{-3} density variation), observed in 3 years of hydrographic data from T3 by *Morison and Smith* [1981]. Of course, a significant fraction of the annual variation is due to the cumulative effect of leads.

4. Comparison With Numerical Experiments

While the experimental results are mainly available for the free convection regime, there are numerical model experiments that give some indication of the types of motions we are likely to encounter for a broader range of lead parameters. *Schaus and Galt* [1973] developed a thermodynamic model of lead convection that ignores the effect of convection on the momentum equation and treats the process as pure diffusion in a constant current. *Kozo* [1983] developed the first model that has the potential to account for the response of the upper ocean in both the forced and free convection modes. It is a nonlinear, time dependent, level model, which can account for horizontal pressure gradients and changes in eddy coefficient with changes in surface buoyancy flux. It has been summarized briefly by *Smith et al.* [1990]. The model is run for a 120-m lead in which the salt flux ramps sinusoidally to a peak magnitude corresponding to an air temperature difference between air and water of about −13.5°C. The model results are given for ice stationary with respect to the water, moving 5 cm s^{-1} parallel to the

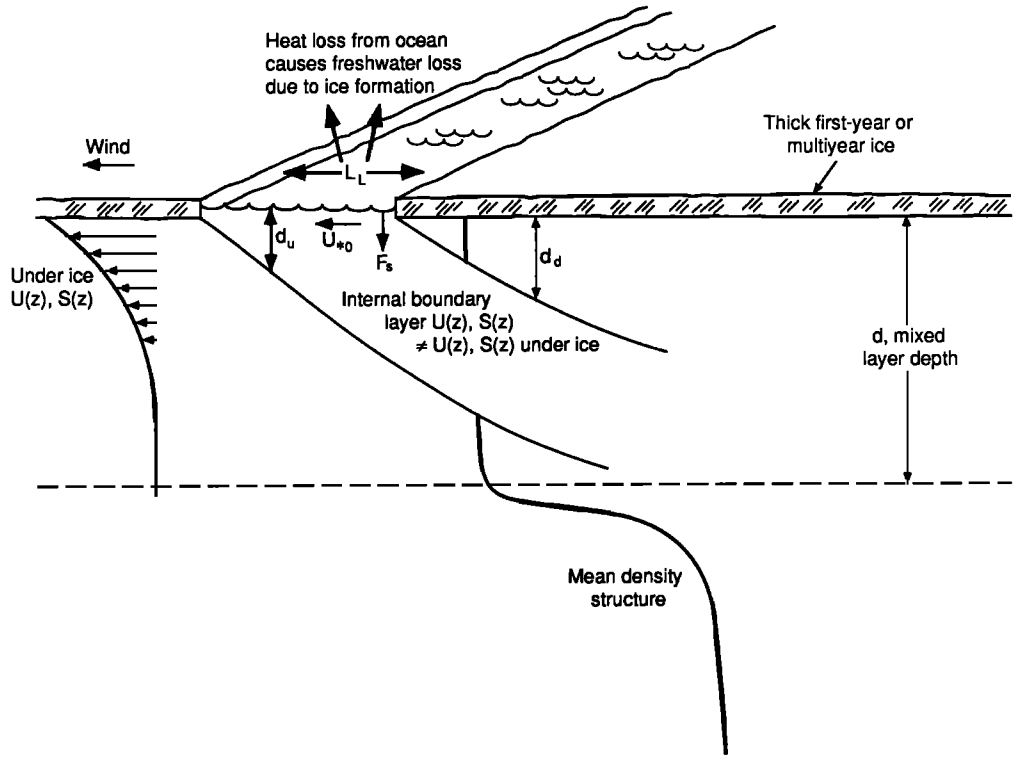

Fig. 15. A conceptual illustration of the effect of a winter lead when there is rapid ice motion. Unstable buoyancy flux at the lead surface modifies the velocity and density in an internal boundary layer downstream of the lead edge. The absolute velocity profile is shown.

lead axis and moving 2.5 and 5.0 cm s^{-1} perpendicular to the lead axis. All the cases produce about 0.1 PSU positive salinity disturbances at the surface in the lead. The salinities decrease linearly to near the mixed layer value at about 5 m. The first two cases produce similar cellular convection patterns on both sides of the lead, with horizontal scales of the order of the lead width and peak currents perpendicular to the lead axis of 2–3 cm s^{-1}. The case with a 2.5 cm s^{-1} ice velocity perpendicular to the lead shows features of cellular convection with 2 cm s^{-1} velocity perturbations, but the upstream cell is eliminated, and the pattern is shifted downstream slightly. With a cross-lead current of 5 cm s^{-1}, the cellular pattern is eliminated. This case has a lead number of 9 and is in the free convection region of Figure 14, so we expect to see some sort of convection driven disturbance in the velocity. Thus Kozo's results suggest forced convection may dominate for some L_o greater than one.

Forced convection under leads has not been examined in detail except for the Dundas Island polynya experiment, for which the tidal turbulent forcing was much greater than usually found in the central Arctic. In a regime where convection is forced, but where the buoyancy contribution is significant for turbulence, the upper ocean structure should look something like the schematic of Figure 15. In this case the process is dominated by turbulent diffusion; the pressure gradient terms of (5) are negligible, and the problem is similar to that of a growing internal boundary layer in the atmosphere downwind of a step change in surface roughness or buoyancy flux. The boundary layer above depth d_u conforms to the boundary conditions at the lead surface. At greater depths the boundary layer conforms to the underice conditions. There is a similar boundary d_d starting at the downstream edge of the lead, above which the underice boundary conditions also apply.

As a first approximation, forced convection can be treated effectively by viewing the solution of a one-dimensional, time dependent numerical model as a steady state, two-dimensional system, using a simple advective transformation suggested by *Mellor et al.* [1986]. Considering (5), (6), and (10) for the steady-state and no-pressure gradient term (forced convection regime), they approximate the equations with

$$u_i \frac{\partial \hat{u}}{\partial x} - if\hat{u} = \frac{\partial}{\partial z}\left[K \frac{\partial \hat{u}}{\partial z}\right] \tag{20}$$

and

$$u_i \frac{\partial S}{\partial x} = \frac{\partial}{\partial z}\left[\alpha K \frac{\partial S}{\partial z}\right] \tag{21}$$

where $\hat{u}$ is the complex velocity $u + iv$. The problem can be converted to a time dependent problem by transforming to a stationary coordinate system. Let $t_* = x/u_i$. Then (20) and (21) are transformed into time dependent, horizontally homogeneous, planetary boundary layer equations:

$$\frac{\partial \hat{u}}{\partial t_*} - if\hat{u} = \frac{\partial}{\partial z}\left[K \frac{\partial \hat{u}}{\partial z}\right] \tag{22}$$

and

$$\frac{\partial S}{\partial t_*} = \frac{\partial}{\partial z}\left[\alpha K \frac{\partial S}{\partial z}\right] \tag{23}$$

The boundary conditions undergo a step change in forcing in t_* when the lead passes over:

$$\frac{\partial \hat{u}(z=0)}{\partial z} = \frac{u_{*o}^2}{K} \text{ and } \frac{\partial S}{\partial z} = \frac{F_s}{\alpha K} \qquad 0 < t_* < L_L/u_i \qquad (24)$$

where u_{*o} and F_s are the specified friction velocity and salt flux at the lead surface. Otherwise, the surface stress and salt flux boundary conditions are those for the under ice boundary layer. The problem can be solved starting at the upstream edge of the lead with $\hat{u}(z)$ and $S(z)$ the same as for the under-ice solution. Then the surface buoyancy flux and surface stress are changed to the lead surface values from $t_* = 0$ to $t_* = L_L/u_i$ and back to the under-ice values for $t_* > L_L/u_i$. In the model scenario we consider a region of ice, containing a large lead, drifting downwind at about 20 cm s^{-1}, perpendicular to the lead axis. The model is similar to that of *McPhee* [1987], but it has been adapted for highly unstable surface buoyancy flux as described in the appendix. It is run to steady state, assuming no salt or heat flux, with a prescribed surface friction velocity, $u_* = 1.5$ cm s^{-1}, and a 40-m deep mixed layer with initial salinity 32 PSU. Beneath the mixed layer is a very stable halocline (with buoyancy frequency 0.02 rad s^{-1}), typical of the central Arctic. The steady, upstream solution serves as the initial condition at the leading (downwind) edge of the lead. At time $t_* = 0$ a freezing rate equivalent to a heat loss of 600 W m^{-2} (an air temperature of −20°C, a wind speed of 10.1 m s^{-1}, and a 60% cloud cover) is applied, producing a source of salinity near the surface.

Two methods have been tried for putting the salt into the ocean: as a salt flux right at the surface and distributing it as a salinity source which falls off exponentially from the surface, reaching $1/e$ of its surface value 2 m below the interface. The results are the same except near the surface where surface injection leads to extremely high surface salinities. Distributing the salt may be more appropriate because the physics at the lead surface may involve complexities not included in the model. For example, most of the freezing may come from frazil crystallization in the upper couple of meters instead of direct congelation growth at the interface. (We do not consider here the interesting question of how frazil ice would affect the turbulence.) Near-surface convection may involve small-scale Langmuir circulation or organized convective plumes. The results shown here are for the distributed salinity method. The salinity source is maintained for 2 h, representing a lead width of about 1.4 km; then surface conditions are returned to their undisturbed, upstream values. In the simulations, turbulence reverts approximately to its upstream state after about two additional hours, that is, about one lead width downstream (upwind).

In the first simulation the surface stress (u_*^2) remains constant during the freezing period. Contours of salinity minus the initial mixed layer value (32 PSU) are shown in Figure 16*a*. Using the advective transformation, $x = t_* u_i$ in a frame of reference following the lead, the $4h$ abscissa represents a section about 2.8 km across, with the lead occupying the left half. The first thing to note is that a fairly strong, statically unstable salinity gradient develops while the surface flux is active. At the trailing edge ($t_* = 2h$), salinity in the surface layer is about 0.02 PSU greater than at the based of the mixed layer. Two distinct depth scales are

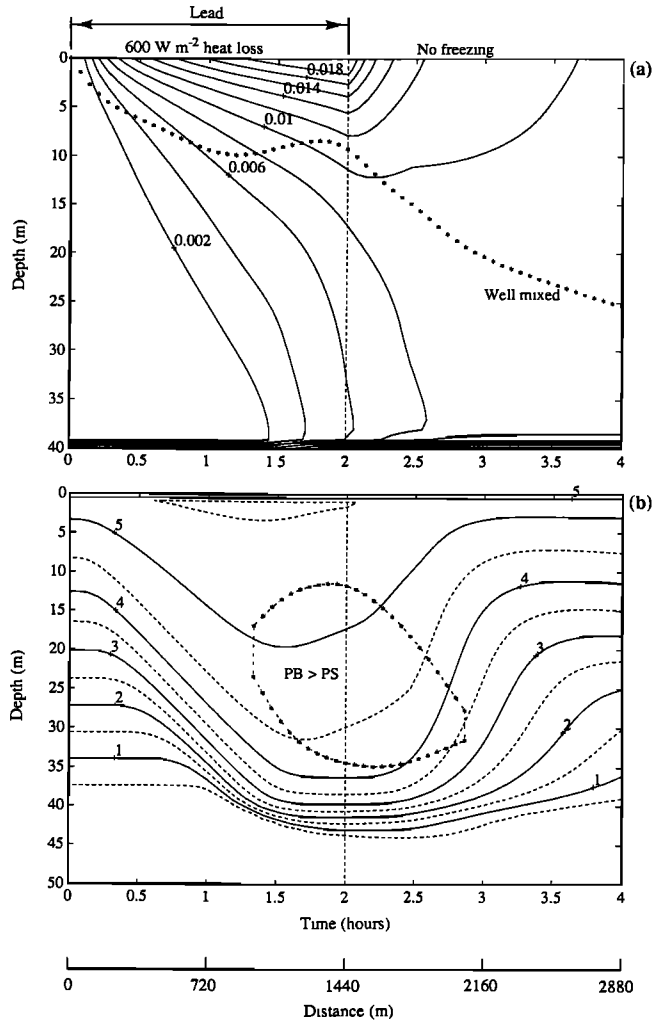

Fig. 16. Internal boundary layer response to freezing in a lead 1440 m across with a 600 W m^{-2} heat loss and a constant surface stress, $u_* = 1.5$ cm s^{-1}. Two horizontal axes are shown: a time axis for a stationary reference frame and a spatial axis for a reference frame moving with the 20 cm s^{-1} ice velocity. (*a*) Salinity disturbance contours (solid line) and e folding depth (line of asterisks). (*b*) Contours of the square root of turbulent kinetic energy q. The region where buoyant production exceeds shear production is bounded by asterisks.

suggested by the salinity structure. The first is the depth above which the main part of the salinity anomaly is contained. This is arbitrarily defined as the level at which the salinity anomaly, relative to the minimum in the mixed layer, is $1/e$ of its value at the surface, as marked by asterisks in Figure 16*a*. Across most of the lead it falls between 5 and 10 m. After freezing stops, this scale increases rapidly but tends to lose its meaning as gradients in the mixed layer disappear. The other scale of interest is the depth to which the surface salinity disturbance penetrates, which can be identified with the internal boundary layer depth d_u in Figure 15. If a convective scale velocity is defined as

$$w_* = \frac{d}{dt_*}(d_u) = u_i \frac{d}{dx}(d_d) \qquad (25)$$

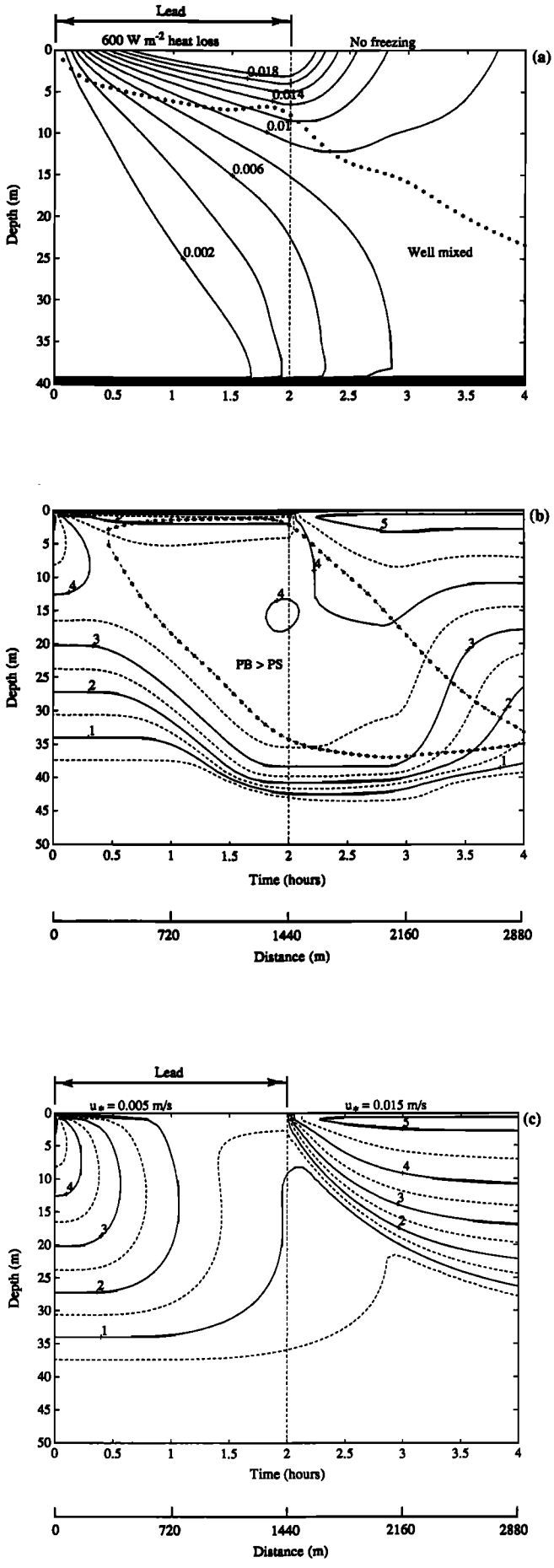

and we approximate it by the slope of the 0.002 PSU salinity anomaly contour (close to the lower limit of detection), w_* is about 0.75 cm s^{-1}, which is half the surface friction velocity.

The effect of freezing on turbulence is demonstrated by contours of the turbulent kinetic energy (TKE) scale velocity, $q = (\langle u'u' \rangle + \langle v'v' \rangle + \langle w'w' \rangle)^{1/2}$ in Figure 16*b*. There is a marked increase in q at mid-depths in response to the destabilizing surface buoyancy flux. The contour plot is suggestive of a highly turbulent wake following the lead (which may help generate internal waves, as described by *Morison* [1980]) and also indicates that it might be easier to detect the lead's impact on the boundary layer by the increase in turbulence rather than by the enhancement of salinity, especially at lower levels.

The enclosed region in the plot indicates where production of TKE by buoyancy (PB = $[(g/\rho)\langle w'\rho' \rangle]$) exceeds production by shear (PS = $\tau \cdot \partial U/\partial z$), that is, where the turbulence regime is classified as free convection. Because u_* remains large, much of the boundary layer is dominated by shear production most of the time, despite the intense buoyancy flux.

Steele et al. [1989] have surmised that surface stress over leads is considerably smaller than over open water. A second model run tested the effect of a large decrease in stress. In this run the friction velocity is changed from its initial value of 1.5 to 0.5 cm s^{-1} when buoyancy flux is active, then back after $2h$. There is surprisingly little change in the salinity structure (Figure 17*a*) from the constant stress case. Note that the slope of the 0.002 PSU contour, which was identified with w_* earlier, is only slightly smaller, indicating that this scale is controlled more by buoyancy flux than surface stress. Figure 17*b* shows that turbulent kinetic energy through the bulk of the boundary layer is quite uniform and not much different from the first run, even though surface stress is reduced by a factor of 9 during freezing. In this case the free convection mode dominates, with the region where PB exceeds PS reminiscent of the plume drawn schematically in Figure 15. A control run, in which stress is reduced over the lead but there is no freezing (Figure 17*c*), demonstrates how effective the strong buoyancy flux is at creating turbulence. At 15 m depth on the trailing edge, for example, turbulent kinetic energy is only about 5% as strong when there is no freezing. The model runs with reduced stress are useful for revealing some of the turbulence and mixing characteristics, but should not be taken too seriously, since they produce large horizontal gradients in near surface currents. In these cases advective terms in the equations cannot be ignored and the simple advective transformation is questionable.

Fig. 17. (Opposite) Internal boundary layer response to freezing in a lead 1440 m across with a 600 W m^{-2} heat loss and u_* = 1.5 cm s^{-1} under the ice and 0.5 cm s^{-1} under the lead. Two horizontal axes are shown: a time axis for a stationary reference frame and a spatial axis for a reference frame moving with the 20 cm s^{-1} ice velocity. (*a*) Salinity disturbance contours (solid line) and *e* folding depth (line of asterisks). (*b*) Contours of the square root of turbulent kinetic energy (cm s^{-1}). The region where buoyant production exceeds shear production is bounded by asterisks. (*c*) Contours of the square root of turbulent kinetic energy as in Figure 17*b* but for no heat flux in the lead.

5. Conclusions and Discussion

The main conclusion of this study is that convection beneath leads is highly variable; it may range from nearly free convection at low ice speeds and low air temperatures to forced convection at high ice velocities and higher air temperatures. On the basis of buoy drift data, *Thorndike and Colony* [1982] estimate the rms ice velocity in the Arctic Ocean is 7 cm s^{-1}. For this speed and a typical springtime air temperature, the lead convection may be transitional, with pressure gradients caused by salinity disturbances and boundary layer turbulence being equally important in the mean momentum balance. Experimental data and model results suggest the velocity disturbances associated with lead convection are about 1 to 5 cm s^{-1}. These appear as jets near the surface and the base of the mixed layer for cross-lead ice velocities less than about 5 cm s^{-1}. The salinity disturbances are about 0.01 to 0.05 PSU, with the maximum occurring at the surface of the lead and decreasing substantially below 5–10 m. This unstable gradient is a unique characteristic of lead convection. The geostrophic currents set up by the lead density disturbances are also of the order of 1–5 cm s^{-1}. The disturbances are greatest for low-ice velocities because the salinity disturbances in the upper ocean are not spread out, but the total transport caused by these currents may be less sensitive to ice velocity.

We have little hard information on the shear stress in the water in leads. *Steele et al.* [1989], in discussing drag partition between ice and open water, indicate that some of the wind stress (typically 16%) over open water goes into making waves rather than producing shear stress. Also, the drag coefficient of wind on water is a quarter that of ice on water. Considering these effects and assuming ice moves at 2% of the wind speed, the surface stress in open water areas should be about 60% of that under ice. This may be increased by the buoyancy flux in the atmosphere. The interior momentum flux in the lead may also be changed by Langmuir circulation associated with the unstable buoyancy flux and small-scale surface waves. The important implication of these factors is that the lead does not simply constitute a change in surface buoyancy flux but a change in momentum flux as well. For the case modeled in this paper the reduction in surface stress in the lead did not have a big effect on the salinity profiles, but this may not always be true. Questions regarding boundary layer modification must be addressed in this light, and near-surface boundary layer phenomena should be examined in future lead experiments.

Finally, we have not devoted much discussion to the situation of rapid ice formation in a stationary lead. In such a case, without any mean advection, the surface salinity disturbance could be quite large, and a pure, three-dimensional, free convection pattern could result. This might involve a cascade of cell sizes as proposed by *Foster* [1972], small cells near the surface merging to form larger cells at depth, the largest cells perhaps scaling with the mixed layer depth. Such a situation would be the most likely to produce penetrative convection such as that shown in Figure 11. It also might be likely to occur in large, stationary shore leads. For these reasons, this situation may be very important in dense water formation and shelf processes, and should receive special attention.

Appendix

In order to accommodate intense buoyancy flux near the surface the first-order turbulence model of *McPhee* [1987] has been modified to include a prognostic equation for q^2, twice the turbulent kinetic energy (TKE) per unit mass. This allows turbulent transport of TKE to play a role in setting the scale velocity for eddy viscosity. If $e = q^2$, the additional scalar equation is

$$e_t = (Ke_z)_z + Q$$

where subscripts denote partial differentiation. Q is a source term for TKE:

$$Q = |\hat{\tau}|^2/K - \alpha_s K N^2 - \varepsilon$$

where $\hat{\tau}$ is the local Reynolds stress, K is the eddy viscosity, N is the local buoyancy frequency (N^2 may be negative), and α_s is the contraction coefficient for salinity. Dissipation, ε, is modeled following the method and notation of *Mellor and Yamada* [1982] as $\varepsilon = q^3/\Lambda_1$, where $\Lambda_1 = (q/u_*)^3 l$ and l is the mixing length scale. The present model is quite similar to the Mellor-Yamada "level 2.5" formulation, except that the mixing length scale is determined diagnostically using the similarity scaling described by *McPhee* [1981, 1987], namely,

$$l = \frac{\xi_N u_*}{f\left(1 + \dfrac{\xi_N u_*}{R_o f L}\right)}$$

where L is Obukhov length; R_c is the critical flux Richardson number, equal to 0.2; f is the Coriolis parameter, ξ_N is a dimensionless constant, equal to 0.05; and $u_* = q/c_1$ is the local scale velocity for turbulent exchange (equivalent to the square root of local Reynolds stress only when shear production equals dissipation). The proportionality constant is obtained from measurements in the ice/ocean boundary layer when buoyancy production is negligible compared with shear production and is found to be about 2.7. As before, eddy viscosity is

$$K = ku_*|z| \quad |z| < l$$

$$K = ku_* l \quad |z| \geq l$$

where k is von Karman's constant, equal to 0.4.

The only other major difference in the present model from that of *McPhee* [1987] is the treatment of surface salinity flux. In the earlier work, the total salinity flux $\langle w'S' \rangle_o$ was treated as a flux boundary condition for the scalar equation

$$S_t = (\alpha_s K S_z)_z \qquad \alpha_s K S_z|_o = -\langle w'S' \rangle_o$$

whereas in the present case the salinity equation is

$$S_t = (\alpha_s K S_z)_z + Q^s \qquad \alpha_s K S_z|_o = 0$$

with

$$Q^s = |\langle w'S' \rangle_o / \lambda_s| e^{-|z|/\lambda_s}$$

where λ_s is the "e folding" depth, equal to 2 m for the present calculations.

Acknowledgments. This work was sponsored by the Naval Postgraduate School, Office of Naval Research (ONR) Chair in Arctic Marine Science, ONR grant N00014-90-J-1077 at the University of Washington, ONR contract N00014-84-C0028 and NSF contract OCE-8923072 at McPhee Research, and ONR grant N00014-90-J-1037 at Oregon State University. The authors wish to thank J. D. Smith for the early insights he shared on the lead problem. They wish to thank M. Steele, D. C. Smith IV, and E. D'Asaro for their helpful comments.

REFERENCES

Anderson, D. L., Growth rate of sea ice, *J. Glaciol.*, *3*, 1170–1172, 1961.

Badgley, F. J., Heat budget at the surface of the Arctic Ocean, in *Proceedings on the Symposium on the Arctic Heat Budget and Atmospheric Circulation*, edited by J. O. Fletcher, pp. 267–277, Rand Corporation, Santa Monica, Calif., 1966. (Available as PB-182433 from Natl. Tech. Inf. Serv., Springfield, Va.)

Bauer, J., and S. Martin, A model of grease ice growth in small leads, *J. Geophys. Res.*, *88*, 2917–2925, 1983.

Cox, G. F. N., and W. F. Weeks, Brine drainage and initial salt entrapment in sodium chloride ice, *CRREL Res. Rep. 345*, Cold Regions Res. and Eng. Lab., Hanover, N. H., 1975.

Cox, G. F. N., and W. F. Weeks, Numerical simulations of the profile properties of undeformed first-year sea ice during the growth season, *J. Geophys. Res.*, *93*(C10), 12,449–12,460, 1988.

Deardorff, J. W., G. E. Willis, and D. K. Lilly, Laboratory investigation of non-steady penetrative convection, *J. Fluid. Mech.*, *35*, part 1, 7–31, 1969.

Estoque, M. A., and C. M. Bhumralkar, Flow over a localized heat source, *Mon. Weather Rev.*, *97*(12), 850–859, 1969.

Fernando, H. J. S., R. R. Chen, and D. L. Boyer, Effects of rotation on convective turbulence, *J. Fluid Mech.*, *228*, 513–547, 1991.

Foster, T. D., Haline convection in polynyas and leads, *J. Phys. Oceanogr.*, *2*(4), 462–469, 1972.

Gow, A. J., D. A. Meese, D. K. Perovich, and W. B. Tucker III, The anatomy of a freezing lead, *J. Geophys. Res.*, *95*, 18,221–18,232, 1992.

Hobbs, P. V., *Ice Physics*, Clarendon, Oxford, 1974.

Kozo, T. L., Initial model results for arctic mixed layer circulation under a refreezing lead, *J. Geophys. Res.*, *88*(C5), 2926–2934, 1983.

Maykut, G. A., Energy exchange over young sea ice in the central Arctic, *J. Geophys. Res.*, *83*, 3646–3658, 1978.

McPhee, M. G., An analytic similarity theory for the planetary boundary layer stabilized by surface buoyancy, *Boundary Layer Meteorol.*, *21*, 325–340, 1981.

McPhee, M. G., A time-dependent model for turbulent transfer in a stratified oceanic boundary layer, *J. Geophys. Res.*, *92*(C7), 6977–6986, 1987.

Mellor, G. L., and T. Yamada, Development of a turbulent closure for geophysical fluid problems, *Rev. Geophys.*, *20*, 851–875, 1982.

Mellor, G. L., M. G. McPhee, and M. Steele, Ice-seawater turbulent boundary layer interaction with melting or freezing, *J. Phys. Oceanogr.*, *16*(11), 1829–1846, 1986.

Morison, J. H., The arctic profiling system, in *Proceedings of a Working Conference on Current Measurement*, pp. 313–317, Coll. of Mar. Stud., Univ. of Delaware, Newark, 1978.

Morison, J. H., Forced internal waves in the Arctic Ocean, Ph.D. thesis, Dept. of Geophysics, Univ. of Wash., Seattle, 1980.

Morison, J. H., and J. D. Smith, Seasonal variations in the upper Arctic Ocean, *Geophys. Res. Lett.*, *8*(7), 753–756, 1981.

Paulson, C. A., and J. D. Smith, The AIDJEX Lead Experiment, in *AIDJEX Bulletin*, 23, vol. 1–8, Univ. of Wash., Seattle, 1974. (Available as PB-230378, from Natl. Tech. Inf. Serv., Springfield, Va.)

Pease, C. H., The size of wind-driven coastal polynyas, *J. Geophys. Res.*, *92*, 7049–7059, 1980.

Schaus, R. H., and J. A. Galt, A thermodynamic model of an arctic lead, *Arctic*, *26*, 208–221, 1973.

Smith, J. D., Lead driven convection in the Arctic Ocean (abstract), *Eos Trans. AGU*, *54*, 1108–1109, 1973.

Smith, J. D., Oceanographic investigations during the AIDJEX Lead Experiment, in *AIDJEX Bulletin*, vol. 27, 125–133, Univ. of Wash., Seattle, 1974. (Available as PB-238574 from Natl. Tech. Inf. Serv., Springfield, Va.)

Smith, J. D., Measurement of turbulence in ocean boundary layers, in *Proceedings of a Working Conference on Current Measurement*, pp. 95–128, Coll. of Mar. Stud., Univ. of Delaware, Newark, 1978.

Smith, S. D., R. D. Muench, and C. H. Pease, Polynyas and leads: An overview of physical processes and environment, *J. Geophys. Res.*, *95*(C6), 9461–9479, 1990.

Steele, M., J. H. Morison, and N. Untersteiner, The partition of air-ice-ocean momentum exchange as a function of ice concentration, floe size, and draft, *J. Geophys. Res.*, *94*(C9), 12,739–12,750, 1989.

Tennekes, H., Free convection in the turbulent Ekman layer of the atmosphere, *J. Atmos. Sci.*, *27*, 1027–1034, 1970.

Thorndike, A. S., and R. Colony, Sea ice motion in response to geostrophic winds, *J. Geophys. Res.*, *87*(C8), 5845–5852, 1982.

Topham, D. R., R. G. Perkin, S. D. Smith, R. J. Anderson, and G. den Hartog, An investigation of a polynya in the Canadian Archipelago, 1, Introduction and oceanography, *J. Geophys. Res.*, *88*, 2888–2899, 1983.

T. B. Curtin, Office of Naval Research, 800 N. Quincy St., Code 1125 AR, Arlington, VA 22217.

M. G. McPhee, 450 Clover Spring Rd., Naches, WA 98937.

J. H. Morison, Polar Science Center, Applied Physics Laboratory, Code HN-10, University of Washington, 1013 NE 40th St., Seattle, WA 98105.

C. A. Paulson, College of Oceanography, Ocean Administration Bldg. 104, Oregon State University, Corvallis, OR 97331.

(Received May 29, 1991;
revised February 28, 1992;
accepted March 16, 1992.)